



Contents lists available at ScienceDirect

Remote Sensing of Environment

journal homepage: www.elsevier.com/locate/rse

Assessing the detectability of European spruce bark beetle green attack in multispectral drone images with high spatial- and temporal resolutions

Langning Huo^{*}, Eva Lindberg, Jonas Bohlin, Henrik Jan Persson

Department of Forest Resource Management, Swedish University of Agriculture Sciences, Sweden

ARTICLE INFO

Edited by Dr. Marie Weiss

Keywords:

Spruce bark beetles
Remote sensing
Green attack
Multispectral imagery
Drone
Forest vitality

ABSTRACT

Detecting disease- or insect-infested forests as early as possible is a classic application of remote sensing. Under conditions of climate change and global warming, outbreaks of the European spruce bark beetle (*Ips typographus*, L.) are threatening spruce forests and the related timber industry across Europe, and early detection of infestations is important for damage control. Infested trees without visible discoloration (green attack) have been identified using multispectral images, but how early green attacks can be detected is still unknown. This study aimed to determine when infested trees start to show an abnormal spectral response compared with healthy trees, and to quantify the detectability of infested trees during the infestation process. Pheromone bags were used to attract bark beetles in a controlled experiment, and subsequent infestations were assessed in the field on a weekly basis. In total, 977 trees were monitored, including 208 attacked trees. Multispectral drone images were obtained before and during the insect attacks, representing different periods of infestation. Individual tree crowns (ITC) were delineated by marker-controlled watershed segmentation, and the average reflectance of ITCs was analyzed based on the duration of infestation. The detectability of green attacks and driving factors were examined. We propose new Multiple Ratio Disease–Water Stress Indices (MR-DSWIs) as vegetation indices (VI) for detecting infestations. We defined a VI range of 5–95% as a healthy tree, and a VI value outside that range as an infested tree. Detection rates using multispectral images were always higher than discoloration rates observed in the field, and the newly proposed MR-DSWIs detected more infested trees than the established VIs. Infestations were detectable at 5 and 10 weeks after an attack at a rate of 15% and 90%, respectively, from the multispectral drone images. Weeks 5–10 of infestation therefore represent a suitable period for using the proposed methodology to map infestation at an early stage.

1. Introduction

As a form of natural disturbance within a forest, insect damage plays an important role in the forest ecosystem. However, climate change and the weather extremes of recent decades have intensified insect outbreaks, causing severe ecological and economic damage. The European spruce bark beetle *Ips typographus* (L.) is an aggressive species across Eurasia, and a major threat to Norway spruce *Picea abies* (L.) forests, a major resource for the European timber industry (Hlásny et al., 2021). Bark beetle outbreaks have been triggered at an unprecedented intensity across Europe since 2015, under conditions of global warming with increasing air temperatures, shifting precipitation patterns, and more frequent windstorms (Senf et al., 2020; Schuldt et al., 2020). During outbreaks in 2018–2019, Sweden reported a 10–11 million m³ timber loss (Huo et al., 2021), and in the Czech Republic it has been estimated

that 260 million EUR of state interventions were needed to compensate for decreased timber prices, excessive workloads, and other cascading effects (Hlásny et al., 2021). It is projected that, by 2030, climate change in Europe will have exacerbated bark beetle disturbances sevenfold compared to 1971–1980 (Seidl et al., 2014). Such biotic threats to the forest ecosystem and forest industry highlight the urgent need for disturbance warning systems, damage control and prevention measures, and an understanding of outbreak mechanisms.

The European spruce bark beetle has a one-year life cycle and usually develops several generations in a year, depending on the temperature conditions. The first swarming starts in the spring when the average temperature exceeds 20 °C (Annala, 1969). The male first excavates a nuptial chamber in the phloem for the gallery construction and then emits aggregation pheromones attracting conspecifics of both sexes to the site (Christiansen and Bakke, 1988). After mating, the female lays

^{*} Corresponding author.

E-mail address: langning.huoslu@slu.se (L. Huo).

<https://doi.org/10.1016/j.rse.2023.113484>

Received 16 September 2022; Received in revised form 16 January 2023; Accepted 22 January 2023

Available online 3 February 2023

0034-4257/© 2023 The Authors. Published by Elsevier Inc. This is an open access article under the CC BY license (<http://creativecommons.org/licenses/by/4.0/>).

eggs in niches along the gallery, and once the larvae hatch, they feed and pupate under the bark and bore dense tunnels. The developmental time from egg to imago is determined by temperature conditions under the bark, and higher temperatures generally shorten the time. A study from Sweden showed that the filial beetles (new generation) started emerging 8 weeks after the brood was initiated, and 50% of the filial beetles had emerged 11 weeks after the brood was initiated (Öhrn et al., 2014). During warm years in northern Europe, the filial beetles usually start a second generation. In central Europe, the second generation is usually fully developed in the same year and can start the third generation during warm years. The adults hibernate and overwinter in the soil or under bark in standing trees during cold years (Öhrn et al., 2014).

While spruce trees can usually fight back, e.g. by releasing resin and defensive chemicals, an intense attack resulting in successful colonization will cause the water transportation in the host trees to be blocked and the trees gradually wither to death within months. At the early infestation stage, the crowns of host trees often stay green for some time after infestation, with no signs of discoloration, hence the term green attack. At this stage, the larvae are still under the bark, therefore, identifying attacked trees at this stage, i.e., early detection, is crucial for damage control if they can be removed from the forest to control the population and reduce attacks by subsequent generations. In the later stages of the infestation, the crowns turn yellow, red, and grey with associated defoliation, and the infestation stages are usually called yellow-attack, red-attack, and grey-attack. Such stages of infestation are common among wood-boring pests (WBPs) such as the European spruce bark beetle (*Ips typographus*), mountain pine beetle (*Dendroctonus ponderosae*), Engelmann spruce beetle (*Dendroctonus rufipennis*), and pine wilt nematode (*Bursaphelenchus xylophilus*) spread by longhorn beetles (*Monochamus* spp.). Identifying attacked trees at the early stage is crucial for damage control if they can be removed from the forest with the larvae under the bark to control the population and reduce attacks by subsequent generations.

Remote-sensing solutions and applications have been developed for monitoring forest pest damage since 1960s (Puritch, 1981). Using remote-sensing data, forest mortality caused by diseases and insects can be identified rapidly and efficiently (Senf et al., 2017; Fang et al., 2021; Zabihi et al., 2021; Atzberger et al., 2020). However, detecting the green attack of WBPs has been challenging because of the subtle spectral changes. For example, the mountain pine beetle (*Dendroctonus ponderosae*), one of the most destructive insects in North America, has an annual life cycle starting in the summer and with the larvae overwintering in the tree and completing the development in the following summer (Coops et al., 2006a). Many studies have been conducted using satellite images to map forest infestations (Coops et al., 2006a; Coops et al., 2006b; White et al., 2007; Hermosilla et al., 2019; Coops et al., 2020). However, detection during the green-attack stage appeared almost impossible using satellite or aerial images (Wulder et al., 2009; Wulder et al., 2006; Puritch, 1981). Similar challenges have also been shown in detecting green attacks of other WBPs, e.g., the Engelmann spruce beetle (*Anoplophora glabripennis*) (Foster et al., 2017) in north American and pine wilt nematode (*Bursaphelenchus xylophilus*) spread by longhorn beetles (*Monochamus* spp.) in Asia (Li et al., 2022a; Zhou et al., 2022; Li et al., 2022b). In recent years, occasional studies showed some potential of using airborne hyperspectral imagery to separate healthy trees with green attacks by the mountain pine beetle (Niemann et al., 2015) and pine wilt nematode (Li et al., 2022c; Yu et al., 2022). In general, for the WBPs mentioned above, almost no studies reported accurate green-attack detection using satellite images, while new opportunities may emerge with very high-resolution images shown by only a few studies (Niemann et al., 2015; Li et al., 2022c; Yu et al., 2022).

For European spruce bark beetle *Ips typographus* (L.) attacks, an increasing number of studies have focused on damage detection and mapping with its increasing outbreaks in Europe these years (Luo et al., 2022; Marvasti-Zadeh et al., 2022). To date, we are not aware of any studies that have presented clear evidence of detecting green attacks

using satellite images, and very few studies detected green attacks using high-resolution airborne or drone images (Honkavaara et al., 2020; Minařík et al., 2021; Bárta et al., 2022). There are two challenges: (1) When using images with too low resolution for the single tree level, e.g., satellite images, the abnormal spectra were difficult to attribute only to the green attack by excluding other factors such as forest structure and vulnerability. (2) Obtaining ground truth on the green-attack stage is challenging, thus, many studies conducted early detection (or detecting early-stage infestation) instead of confirming the green-attack stage. The early detection should be conducted before 8–12 weeks of infestation, when the larvae are still inside the bark, while studies often simply it as before the red-attack stage and is often assumed according to the season, e.g. from May to July (Lausch et al., 2013; Fassnacht et al., 2014; Immitzer and Atzberger, 2014; Tanase et al., 2018; Latifi et al., 2014; Huo et al., 2021).

So far, few studies of satellite imagery have presented the abnormal spectrum during green attacks by excluding the influences from the variation of forest structures and vulnerability. Many studies have presented the spectral differences between healthy and early-infested trees using satellite images of middle to high resolution, such as the Landsat series (Abdullah et al., 2019a; Latifi et al., 2014), RapidEye (Abdullah et al., 2019c; Ortiz et al., 2013), SPOT series (Latifi et al., 2014; Abdullah et al., 2019c), Sentinel-2 (Huo et al., 2021; Bárta et al., 2021; Abdullah et al., 2019b; Yang, 2019), and Worldview-2 (Immitzer and Atzberger, 2014), as well as aerial images (Lausch et al., 2013; Fassnacht et al., 2014; Einzmann et al., 2021; Hellwig et al., 2021). However, these studies could not exclude the possibility that the spectral differences existed before the attacks, thus, no conclusion could be made on the detectability of the green attack. Previous studies have presented such a possibility, for example, in the studies by Huo et al. (2021) and Bárta et al. (2021), the spectral differences between the healthy and attacked trees already existed before the attacks, and the spectral differences maintained but not increased during the green-attack phase. Another study also confirmed no abnormal spectrum during the green-attack stage using healthy and attacked samples without spectral differences before attacks in Sentinel-2 images (Huo et al., 2022). Therefore, the spectral differences which existed both before and during green attacks in satellite images, either caused by vulnerable forests or variations of forest structures, cannot support the conclusion that green attack is detectable.

Ground data availability is another limitation to concluding the detectability of the green attack. Some studies have identified attacked areas later in the season and made assumptions about the green-attack period without sufficient validation by field inventories. For example, green attacks were assumed in June and July (Lausch et al., 2013; Fassnacht et al., 2014; Immitzer and Atzberger, 2014; Tanase et al., 2018; Latifi et al., 2014; Huo et al., 2021), or 1–6 months before discoloration (Bárta et al., 2021). Such assumptions may lead to a misconception of detecting green attacks while detecting trees with discoloration attacked from an earlier year or earlier swarming. Other studies have conducted one-time data acquisition with combinations of green, yellow, red, and grey attacks, resulting in a limited sample size for green-attack trees (Hellwig et al., 2021; Klouček et al., 2019; Honkavaara et al., 2020). Elsewhere, healthy and declined trees have been identified without defining a specific phase (Näsi et al., 2015; Junttila et al., 2022; Näsi et al., 2018; Minařík and Langhammer, 2016). None of these studies have identified the start of an attack, thus no conclusion can be drawn about how soon an infestation has been detected after an attack.

Using very high-resolution images and analyzing the spectrum only from the tree crowns, i.e., at the single-tree level, is one of the solutions to reduce the influences from the forest structure. Drone images (unmanned aerial vehicles, UAV) usually have a centimeter-level resolution, with multispectral or hyperspectral reflectance data covering many pixels per tree crown. These images support spectral analyses at the individual-tree level, and their spectra are less disturbed than satellite

images by the vitality and species of neighboring trees, canopy gaps, and low forest vegetation. The development of drones and drone-mounted sensors has facilitated research on mortality mapping (Junntila et al., 2022; Klouček et al., 2019; Minařík et al., 2021; Näsi et al., 2015; Näsi et al., 2018; Minařík et al., 2020).

To date, we are aware of only three studies conducted at the single-tree level with field inventory to validate the green attack (Honkavaara et al., 2020; Minařík et al., 2021; Bárta et al., 2022). Honkavaara et al. (2020) detected 64% of green-attack trees and Minařík et al. (2021) separated healthy and green-attack trees with the F-score being 0.60–0.63 using Random Forest classification. The latter study also achieved classification with an F-score of 0.83 using deep learning, but the data size was insufficient for training a transferable convolutional neural network model avoiding overfitting to the used dataset. No detection accuracy was presented in the study by Bárta et al. (2022), but the study presented significantly different 25th and 75th percentiles of reflectance between healthy and attacked trees 23 days after the attack began, based on 75 attacked trees. The conclusion drawn from this was that infested trees should be detected and removed within 4–6 weeks of infestation. Unfortunately, this study did not quantify the separability or classification accuracy between healthy and attacked trees, and the detectability was tested monthly without a transition period between “undetectable” and “detectable”.

Since infested, tree vitality declines along a continuum, but the process has been simplified as green, yellow, red, and grey phases of attacks based on crown discoloration (Luo et al., 2022). Although studies have identified green-attack trees (Honkavaara et al., 2020; Minařík et al., 2021), it is unclear how long the infested trees in these studies had been in the green-attack phase, and more accurate timings for detectability are needed to plan effective sanitation cutting. Several difficulties need to be overcome to address these issues: (1) green attack is challenging to find in the field, thus limiting sample sizes and analyses; and (2) frequent field observations are needed to identify the start of an attack.

Whether green attacks can be detected using remote sensing is a fundamental research question to further develop forest monitoring and early warning techniques. Assessing detectability during the infestation process is also crucial for arranging efficient and effective sanitation cutting before brood emergence, and contributing to damage control. This study aims to answer whether it is possible to detect green attacks, how early the infestations can be detected, and what is the detection accuracy, i.e., detectability of green attacks. We used revisiting multi-spectral drone imagery to focus on the crown reflectance and avoid noise

due to other factors (e.g., ground visibility) in the forest. We conducted extensive fieldwork to collect the starting time of the infestations and the stages of the infestations during a growing season. Supported by repeated, very high-resolution image acquisitions and field inventory, we aim to confirm whether green attacks are detectable, and, for the first time, quantify a weekly detectability curve of infestations since being attacked. This study also proposes improved methods for early detection using very high resolution multispectral imagery.

2. Materials and methods

2.1. Study area and field observations

The study area is located in Remningstorp, Sweden (58°27′18″N, 13°39′8″E, Fig. 1a), a hemiboreal forest estate covering 1602 ha. The forests in this area are mainly Norway spruce (*Picea abies* [L.] Karst) and Scotch pine (*Pinus sylvestris* [L.]) managed for wood production. It is an experimental forest and our group has sample plots with inventory of forest attributes scattered in the estate. In the study area, bark beetle attacks had occurred in some stands from 2018 to 2020.

The field observations and data collection were conducted from April to October 2021. In the study area, we first selected six stands fulfilling (1) having infestations from 2020, (2) the volume of spruce was larger than 80%, (3) mature forest, and (4) sufficiently large area for setting up four plots with 15 m radius. In each stand, four plots with a 15-m radius were set up to be attacked plots (Fig. 1), prioritizing (1) not damaging the long-term plots used by other studies that were sampled in grids over the estate, (2) not having dead trees or attacked trees from previous years in the plots, (3) not having other tree species, and (4) close to a group of trees attacked in 2020. Not all of these criteria could be fulfilled, but we prioritized the first ones.

To ensure beetle colonization, pheromone bags were attached to a tree close to the center of each plot (denoted as central trees), about 2 m above ground. The pheromone bags contain Phero-X-Lure IT simulating the aggregation of pheromones emitted by bark beetles. It can attract conspecifics to the site and cause an attack on surrounding trees. Such pheromone bags have been commonly used for monitoring beetle swarming and used in the management of bark beetle outbreaks (Ozcan et al., 2014; Öhrn et al., 2014; Meurisse et al., 2008; Schroeder, 2013). The pheromone bags used in this study can last at least 14 weeks, while we used them from week 16 (April 5) to week 22 (May 31). We removed the pheromone bags from the central trees at the end of May, two weeks after the first swarming, so the parental beetles could attack other trees

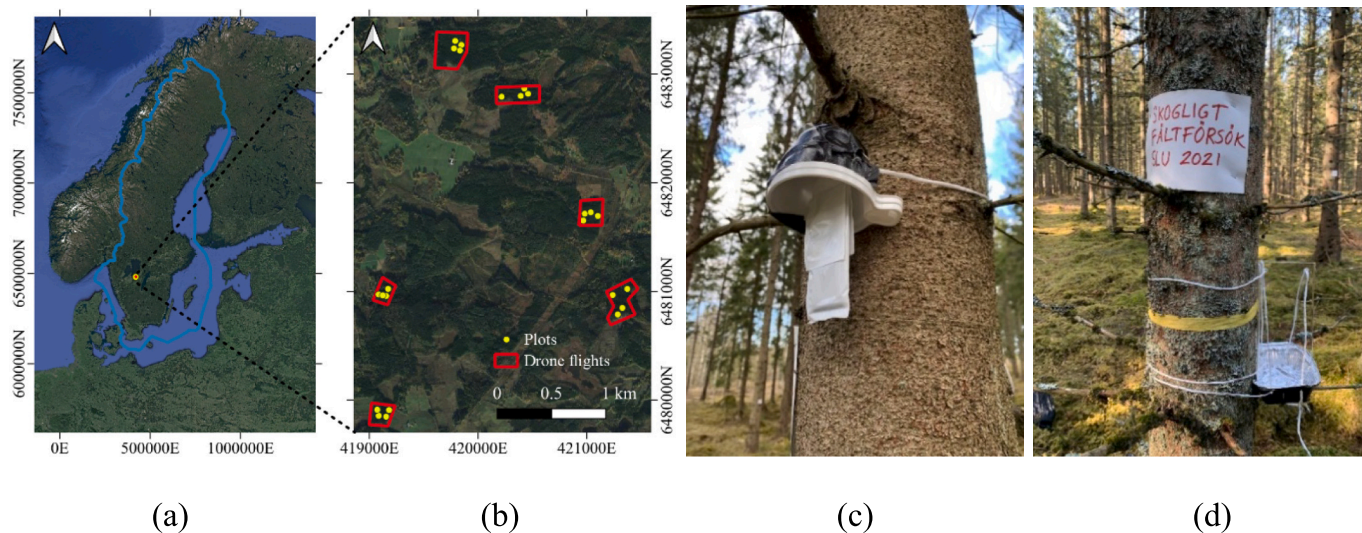


Fig. 1. The study area in Remningstorp, Sweden (a), stands and plots (b), a pheromone bag (c) and a flight interception trap for bark beetles (d) on the central tree of a plot.

to initiate the sister broods (Öhrn et al., 2014), and more data from the attacked trees could be collected. On each central tree below the pheromone bag, we also attached a flight interception trap to monitor the swarming and indicate the potential attacks. More information on the traps is presented in Appendix A.

The locations and diameters at breast height (DBH) of the individual trees were measured in April. The mean DBH of the sampling trees was 27.9 cm (Appendix B). Field observations of the infestation symptoms were conducted weekly from week 16 (the week commencing April 5 in 2021) to week 33 (August 16), and during week 42 (October 18). Symptoms of infestation were visually assessed by the same field assistant every week, as consistently as possible. The recorded symptoms included:

- (1) resin flow at three levels, i.e., none, < 30 spots, > 30 spots;
- (2) number of holes in the bark at three levels, i.e., none, < 30 spots, > 30 spots;
- (3) bark damage at three levels, i.e., none, minor damage, major damage with exfoliated bark;
- (4) discoloration of the tree crown at four levels, i.e., green, yellow, red, and grey.
- (5) defoliation at four levels, i.e., 0–25%, 25–50%, 50%–75%, and 75%–100%.

In week 20 (May 17), bark beetles started swarming. They were caught in the traps, and entrance holes appeared in the bark of some trees. We determined the beginning of an attack when the entrance holes of bark beetles appeared in the bark. In total, 977 trees were monitored, 208 of which were attacked by bark beetles during two swarmings (Fig. 2a). During the first swarming, 151 trees were attacked from week 20 to week 23, and 10 trees were attacked from week 24 to 29. During the second swarming, 21 trees were attacked during week 30, and 26 trees were attacked during weeks 34 to 42; the latter were not included in the analyses because no field observations took place between weeks 33 and 42. The spectral characteristics of trees attacked during the first and second swarming were analyzed separately to explore possible differences.

2.2. Drone image acquisition

A MAIA S2 multispectral camera (SAL Engineering S.R.L. and EOP-TIS S.R.L., Italy) was used, mounted on a DJI Matrice 210 RTK drone (Fig. 3). The MAIA camera has nine sensors with a resolution of 1280 × 960 pixels, and the pixel size was 3.75 μm × 3.75 μm, resulting in an active area of 4.8 mm × 3.6 mm. Each sensor was linked to a band-pass filter that defined the wavelength range (band). We used the MAIA camera with a filter that matched the bands of the Sentinel-2 satellite at wavelengths ranging from 390 nm to 950 nm (Table 1). The camera was

equipped with a MAIA Incident Light Sensor (ILS) that measured the ambient light level for each band, which was then used to calculate the true reflectance ratios. It had an integrated 6-axis inertial unit for motion processing, and a Global Navigation Satellite System (GNSS) receiver that provided a timestamp and position information for each image. The drone with the MAIA camera was flown at 80 m above the ground, with an 80% forward and side overlap. The flight height provided a nominal ground sampling distance (GSD) of 4 cm. Four radiometric reference targets (1 m × 1 m) were installed to transform the image data to reflectance.

The drone images were acquired during the following weeks of the year.

Week 19 (May 10–16). Before the bark beetle attacks began and the trees were healthy.

Week 25 (June 21–27). After the attacked trees had experienced 1–5 weeks of infestation.

Week 33 (August 16–22). The trees attacked by the first swarming (attacked before week 25) had experienced 9–13 weeks of infestation, and 40% of them were discolored. The trees attacked in the autumn (attacked after week 25) had experienced 3–6 weeks of infestation without any discoloration observed in the field.

Week 42 (October 18–24). The trees attacked in the spring (attacked before week 25) had experienced 18–21 weeks of infestation, and most of their crowns were yellow or red. The trees attacked in the autumn (attacked after week 25) had experienced 12–15 weeks of infestation, with 37% of them discolored, based on field observations (Fig. 4).

2.3. Drone-image processing

For each exposure point, the MAIA camera generated nine raw images, one for each spectral band. Post-processing of the raw images was carried out using the MAIA image-processing software and included the following corrections.

- (1) A geometric correction for each single-band raw image using the camera calibration parameters included for each sensor.
- (2) Co-registration of each spectral band image and generation of multi-band images based on a reference image using pixel-by-pixel convergence. The no-data borders of images were cropped.
- (3) Radial radiometric correction of the border effects of the images as a result of lens curvature.
- (4) Radiometric correction based on the ILS.

The post-processed images (Fig. 5a) were then used to generate orthomosaic images (Fig. 5b) using Agisoft Metashape Professional (Version 1.7.2, Copyright 2021 Agisoft LLC.), including aligning photos, optimizing alignment, building a dense cloud, building digital surface models (DSMs), and building orthomosaics. The orthomosaic images

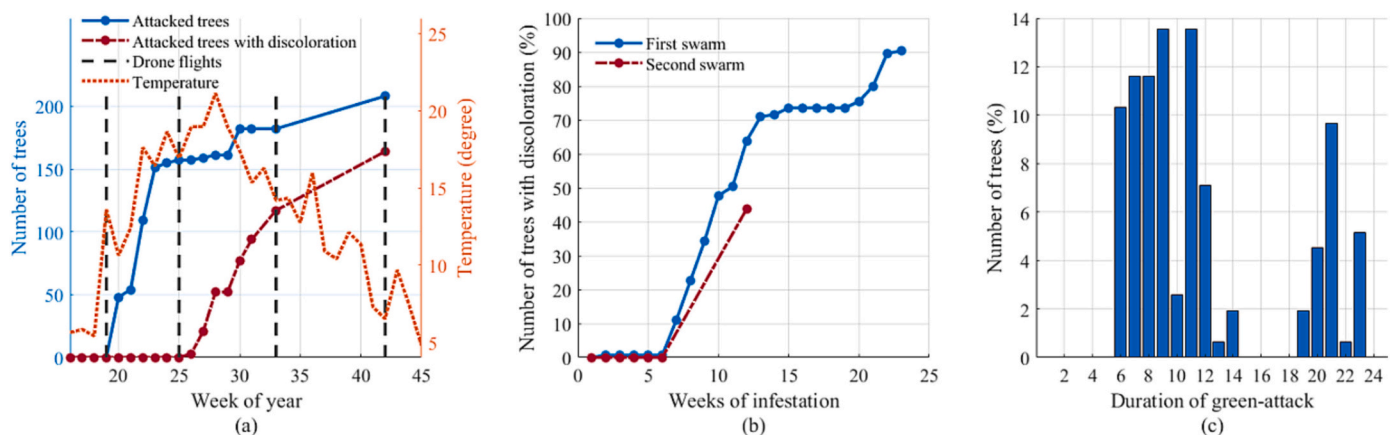


Fig. 2. The number of discolored crowns during the growing season (a), the proportions of trees with discolored crowns at different weeks of infestation (b), and the duration of the green attack. (For interpretation of the references to colour in this figure legend, the reader is referred to the web version of this article.)

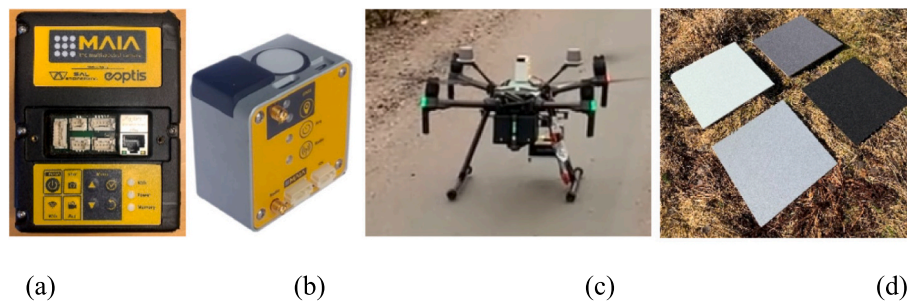


Fig. 3. The MAIA camera, MAIA ILS, DJI Matrice 210 RTK, and the radiometric reference targets.

Table 1
Summary of the MAIA S2 multispectral camera specifications.

Band no.	Colour	Center wavelength (nm)	Bandwidth (nm)
1	Violet	443	20
2	Blue	490	65
3	Green	560	35
4	Red	665	30
5	Red-edge 1	705	15
6	Red-edge 2	740	15
7	Red-edge 3	783	20
8	Near infrared (NIR) 1	842	115
9	NIR 2	865	20

were radiometrically transformed to reflectance (Fig. 5c) using the known reflectance of the radiometric reference targets, and manually georeferenced to an aerial image (acquired in 2016 and provided by the Swedish Land Survey) that covered the study area, with a 0.25-m resolution.

2.4. Individual tree crown delineation

Individual tree segmentation was conducted using the green band (band 3), and the generated segments were used for all bands. The local maxima in the images were detected as treetops and used for marker-controlled watershed segmentation (Fig. 6a), conducted using the SegmentTrees tool in the Lidar Toolbox in Matlab (MathWorks, Inc., 2021). Segmentation usually resulted in segments that contained both tree crowns and the surrounding canopy gaps. Thus, we defined pixels $> Th_{green}$ reflectance in the green band as the tree crowns and masked out the rest. We used $Th_{green} = 0.015$ and conducted a sensitivity analysis on Th_{green} to reveal its influence on infestation detection (Appendix C). The segments were linked with the tree identification numbers and field infestation records by matching the local maxima within the segments with the spruce locations measured in the field (Fig. 6b). For this step, the local maxima were linked to all possible field measurements and the pairs with smaller distances prioritized until all the local maxima had been paired with field measurements.

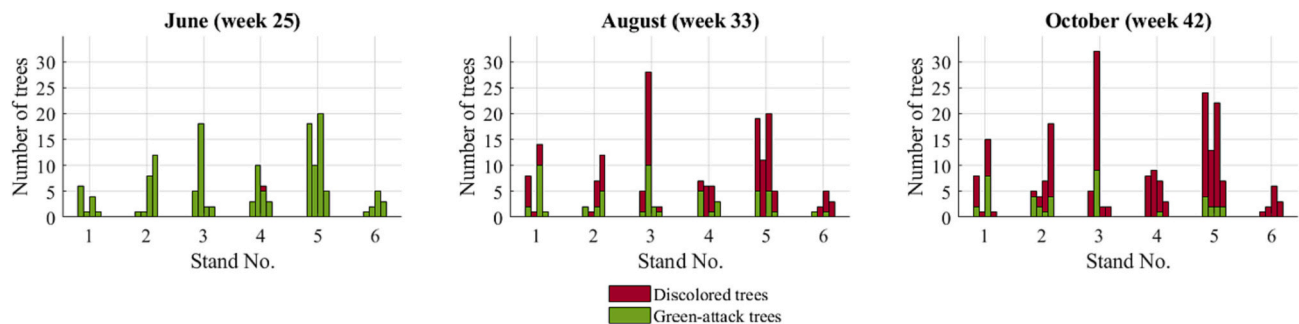


Fig. 4. The number of infested trees in each plot (single bars) and stand in June, August, and October, when the drone images were acquired. The red bars indicate discolored trees and the green bars indicate green-attack trees. (For interpretation of the references to colour in this figure legend, the reader is referred to the web version of this article.)

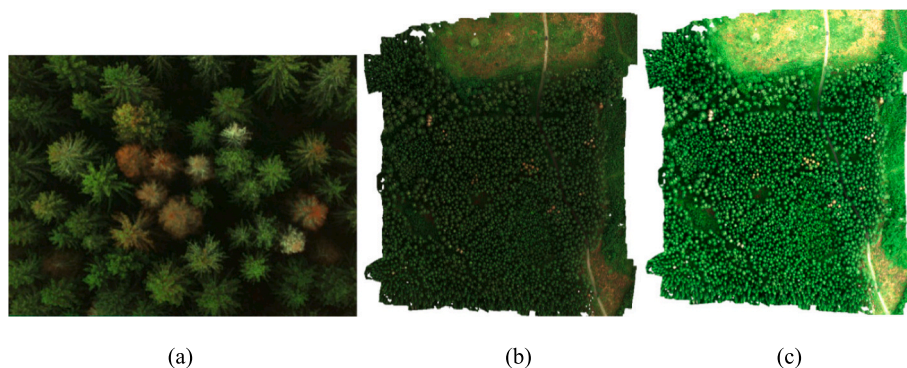


Fig. 5. A post-processed multi-band single image from August (a), and an orthomosaic image before (b) and after (c) radiometric correction using the radiometric reference targets. The images are illustrated with the red (665 nm), green (560 nm), and blue (490 nm) bands.

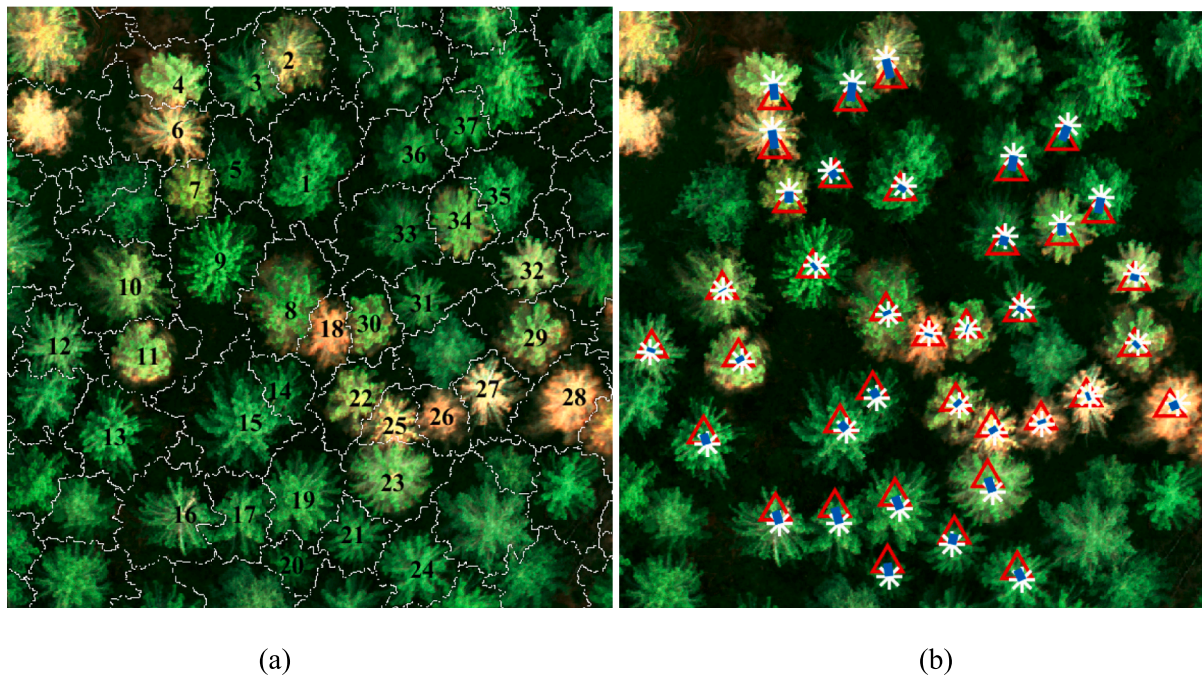


Fig. 6. Segmentation of individual tree crowns from an orthomosaic image taken in August, showing the red-green-blue (RGB) bands. (a) The results of marker-controlled watershed segmentation. (b) Local maxima detection (white stars) and tree locations measured in the field (red triangles). Blue lines indicate the linked pairs of local maxima and field data. (For interpretation of the references to colour in this figure legend, the reader is referred to the web version of this article.)

2.5. Spectral and temporal analyses

To calculate the spectra of a tree, the pixel values within a tree crown segment were averaged for each band. Spectral curves of healthy and attacked trees were drawn by presenting the median, 5th, and 95th percentiles, and were derived for May, June, August, and October. To identify the temporal characteristics of an infestation, we grouped trees by the duration of infestation (denoted as tree groups), and analyzed the spectral differences between the tree groups. The spectra of trees attacked by the first swarming (attacked before week 25) and second swarming (attacked at week 30) were analyzed separately, to determine whether they presented different temporal characteristics. Spectral differences were tested using a two-sided Wilcoxon rank-sum test, comparing the null hypothesis that data from the two groups were samples from a continuous distribution with equal medians, against the alternative that they were not. The test assumed that the two groups were independent, and the differences were tested at the $p < 0.01$ and $p < 0.001$ levels. We also quantified the separability of the infestations by determining the kappa coefficient after classification using linear discriminant analysis (LDA).

2.6. Developing vegetation indices

The bark beetle attacks affect the trees' water transportation system, leading to water-stress symptoms, i.e., decreasing water content, loss of chlorophyll, and structural changes in the spongy mesophyll (Zabihi et al., 2021). Based on the spectral signature changes after attacked, we first calculated four ratio indices that should theoretically increase when a tree is under water-related stress (Penuelas et al., 1995; Gamon et al., 1997); (Ehammer et al., 2010):

- the ratio of the red and green bands ($R_1 = \frac{Red}{Green}$) (Red/Green Ratio)
- the ratio of the red-edge and green bands ($R_2 = \frac{Red_edge1}{Green}$)
- the ratio of the two red-edge bands with 705 nm and 783 nm ($R_3 = \frac{Red_edge1}{Red_edge3}$)

- the ratio of the NIR and red-edge bands with 865 nm and 783 nm ($R_4 = \frac{NIR2}{Red_edge3}$)

We then tested whether using multiple ratios could magnify any differences between the infested and healthy trees, using Eqs. 1–4:

$$MR_DSWI1 = R_2 \times R_3 = \frac{Red_edge1}{Green} \times \frac{Red_edge1}{Red_edge3} \quad (1)$$

$$MR_DSWI2 = R_2 \times R_3 \times R_4 = \frac{Red_edge1}{Green} \times \frac{Red_edge1}{Red_edge3} \times \frac{NIR2}{Red_edge3} \quad (2)$$

$$MR_DSWI3 = R_2 \times R_3 \times R_1 = \frac{Red_edge1}{Green} \times \frac{Red_edge1}{Red_edge3} \times \frac{Red}{Green} \quad (3)$$

$$MR_DSWI4 = R_2 \times R_3 \times R_4 \times R_1 \\ = \frac{Red_edge1}{Green} \times \frac{Red_edge1}{Red_edge3} \times \frac{NIR2}{Red_edge3} \times \frac{Red}{Green} \quad (4)$$

The band combinations were proposed based on the observation of spectral signature changes (Section 3.2.2) and supported by the theoretical radiation changes during the decline of tree vitality. The chlorophyll loss should be revealed by less absorption in the red band compared with the green band ($\frac{Red}{Green}$), i.e. the Red/Green Ratio index, and indicates photosynthetic radiation (Penuelas et al., 1995; Gamon et al., 1997). The red-edge bands with wavelengths around 700 nm – 720 nm are commonly used for indicating water stress of vegetation, and we used both the green and the Red-edge3 bands respectively to normalize the reflectance of the red-edge band to reduce the influences of tree height and shadows. The ratio of the NIR and red-edge bands, i.e., NIR/Red-Edge Ratio Index 1, has also been used for estimating photosynthetic active radiation and leaf area index (Ehammer et al., 2010). The spongy mesophyll changes should be revealed by less absorption in the NIR bands compared with Red-edge3 bands ($\frac{NIR2}{Red_edge3}$). The combination of the two bands has also been used in Normalized Difference Red-edge Index 3, indicating the post-fire conditions of forests. This

study used simple ratios between two bands and multiplied them as new VIs to quantify the decline of tree vitality after attacked.

The performance of the MR-DSWIs was compared with other vegetation indices (VIs), as listed in Table 2.

2.7. Detection of infestation and analysis of the detectability

The detection of infestation was built on the threshold of each VI. We assumed that healthy and infested trees would have similar VI distributions before an attack (denoted as a healthy VI range) and that, as the infestations progressed, infested trees would gradually show abnormal spectra and VI values.

We calculated the healthy VI range using our healthy samples (5% and 95% percentiles, to exclude extreme values), and detected an infested tree when the VI value for the tree was outside the healthy range. Detection rates were calculated for trees after different periods of infestation to show the detectability. We also compared the detection rates between using different VIs.

Table 2
Details of the vegetation indices (VIs) used.

No.	Abbr.	Name	Definition for MAIA S2 / Sentinel-2 bands (https://www.indexdatabase.de/)	References
1	MR-DSWI1	Multiple Ratio Disease–Water Stress Index 1	$\frac{Red_edge1}{Green} \times \frac{Red_edge1}{Red_edge3}$	Proposed in this study
2	MR-DSWI2	Multiple Ratio Disease–Water Stress Index 2	$\frac{Red_edge1}{Green} \times \frac{Red_edge1}{Red_edge3} \times \frac{NIR2}{Red_edge3}$	Proposed in this study
3	MR-DSWI3	Multiple Ratio Disease–Water Stress Index 3	$\frac{Red_edge1}{Green} \times \frac{Red_edge1}{Red_edge3} \times \frac{Red}{Green}$	Proposed in this study
4	MR-DSWI4	Multiple Ratio Disease–Water Stress Index 4	$\frac{Red_edge1}{Green} \times \frac{Red_edge1}{Red_edge3} \times \frac{NIR2}{Red_edge3} \times \frac{Red}{Green}$	Proposed in this study
5	NDRE2	Normalized Difference Red-edge Index 2	$\frac{Red_edge3 - Red_edge1}{Red_edge3 + Red_edge1}$	(Barnes et al., 2000)
6	NGRDI	Green-Red Difference Index	$\frac{Green - Red}{Green + Red}$	(Tucker, 1979)
7	NDVI	Normalized Difference Vegetation Index	$\frac{NIR2 - Red}{NIR2 + Red}$	(Rouse et al., 1973)
8	GLI	Green Leaf Index	$\frac{(Green - Red) + (Green - Blue)}{(Green + Red) + (Green + Blue)}$	(Louhaichi et al., 2001)
9	PBI	Plant Biochemical Index	$\frac{NIR2}{Green}$	(Abdullah et al., 2019c)
10	GNDVI	Normalized Difference Vegetation Index	$\frac{NIR2 - Green}{NIR2 + Green}$	(Gitelson and Merzlyak, 1998)
11	CIG	Chlorophyll Index Green	$\frac{NIR2}{Green} - 1$	(Gitelson et al., 2003)
12	CVI	Chlorophyll Vegetation Index	$\frac{NIR2 \times Red_edge1}{Green \times Green}$	(Hunt et al., 2011)
13	NDRE3	Normalized Difference Red-edge Index 3	$\frac{NIR2 - Red_edge3}{NIR2 + Red_edge3}$	(Navarro et al., 2017)

3. Results

3.1. Individual tree segmentation

After pre-processing the drone images, we segmented individual-tree crowns as areas of interest (Fig. 7). This section presents results related to the quality and the segmentation of the drone images. The orthomosaic images from May, June, and August included 92% to 98% of the trees, apart from the October image of Stand 2, which was influenced by wind and included only 86% of the trees (Table 3). During the four drone flights, we captured the status of trees after 1 to 22 weeks of infestation, in total obtaining 486 single-tree images of trees infested for different time periods (Fig. 7, used as samples). Different samples could come from the same tree but represent different periods of infestation. We grouped the samples by infestation duration, and presented the average spectral curves for the different groups. Eleven groups had >20 samples and were used for the spectral analysis. They were infested for 2, 3, 5, 10, 11, 13, 19, 20, and 22 weeks during the first swarming, and 3 and 12 weeks during the second swarming (Fig. 8). The rest of the groups had too few samples to represent infestation status and spectral features.

3.2. Spectral and temporal changes during infestation

3.2.1. Individual bands and temporal features

The attacked trees showed the following spectral differences compared with healthy trees (Fig. 9 and Table 4). The May image did not show any significant spectral differences (i.e., $p < 0.001$) between healthy trees and trees attacked in June. The median of violet, blue, green, red, and red-edge1 bands increased after infestation, while red-edge2, NIR 1, NIR2, and NIR3 decreased after infestation. Only the red-edge1 and green bands showed significant differences in the June image between healthy and attacked trees. Only the red-edge1 showed significant differences ($p < 0.01$) after 3 weeks of infestation during the first swarming, with no significant differences for infestations during the second swarming. Only the red-edge1 and green bands showed significant differences 5 weeks after attacked by the first swarming. The red-edge2 and all the NIR bands did not show any significant differences at 12 weeks of infestation during the second swarming. All the other bands showed significant differences after 10 weeks of infestation during both attacks.

3.2.2. Spectral signatures

As the infestations progressed, the spectral signatures gradually lost the characteristics of a typical vegetation spectrum (Fig. 10). The spectral absorption by chlorophyll became weaker, increasing the ratio of red and green bands ($R_1 = \frac{Red}{Green}$) (Red/Green Ratio). The green–red-edge–NIR curve became flatter, increasing the ratio of red-edge and green bands ($R_2 = \frac{Red_edge1}{Green}$), and the ratio of NIR and red-edge bands ($R_3 = \frac{Red_edge1}{Red_edge3}$) (NIR/Red-Edge Ratio Index 1). The spectral absorption by the spongy parenchyma became weaker, increasing the ratio of NIR bands at 860 nm and 780 nm ($R_4 = \frac{NIR2}{Red_edge3}$).

3.3. Detection rates

We examined the detection rates using R_1, R_2, R_3, R_4 as indices, and classified a tree as infested when the index value was smaller or larger than the 5% or 95% percentile values of healthy trees. Fig. 11(a) shows that, by comparing $R_1, R_2, R_3,$ and $R_4, R_2 \left(\frac{Red_edge1}{Green} \right)$ was the best for detecting infestations at 10–12 weeks, but the detection rates at 2–5 weeks were lower and did not increase when more visible discoloration developed during later infestation stages. $R_3 \left(\frac{Red_edge1}{Red_edge3} \right)$ and $R_1 \left(\frac{Red}{Green} \right)$ identified more infestations at 2–5 weeks and 19–22 weeks,

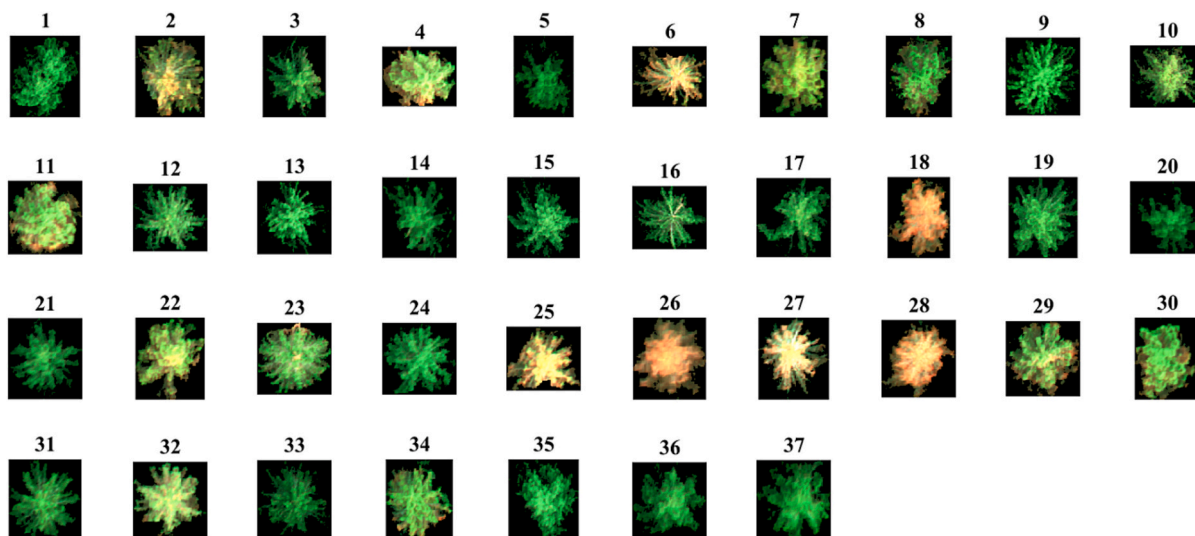


Fig. 7. True colour RGB images of individual trees in October, including healthy, green-attack, and discolored trees. The black backgrounds were not part of the tree crowns and were masked out. (For interpretation of the references to colour in this figure legend, the reader is referred to the web version of this article.)

Table 3

The number of trees based on the inventory and segmentation of the drone images from the four flights (May, June, August, October).

Category	From inventory	From the image taken in							
		May		June		August		October	
		Number	%	Number	%	Number	%	Number	%
Healthy	769	718	93	723	94	710	92	661	86
Attacked	208	201	97	204	98	199	96	179	86
Total	977	919	94	927	95	909	93	840	86

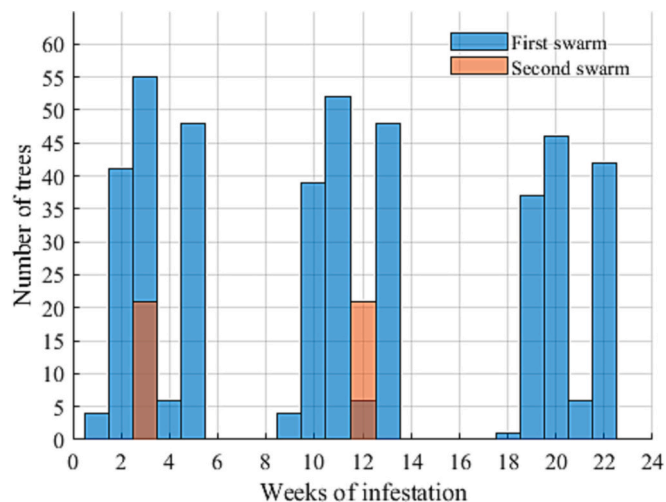


Fig. 8. The number of trees representing different durations of infestation.

respectively, with R_3 showing higher detection rates than R_1 . We therefore assumed that multiplying R_2 and R_3 would result in better detection rates at both early and later stages of infestation. We tested this hypothesis by estimating the detection rates of the MR-DWSIs. The results (Fig. 11b) verified that $R_2 \times R_3$ achieved a higher detection rate than using R_2 or R_3 separately, while $R_2 \times R_3 \times R_4$, rather than $R_2 \times R_3 \times R_1$ or $R_2 \times R_3 \times R_4 \times R_1$, showed an even higher detection rate than $R_2 \times R_3$.

Comparing these with existing VIs, MR-DSWI2 achieved the highest detection rates, followed by MR-DSWI1. MR-DSWI3 and MR-DSWI4

achieved higher detection rates than all the other VIs except NDRE2 at 11 weeks of infestation (Fig. 10, Appendix D). Among the established VIs, NDRE2 achieved the best detection of infestations, followed by NGRDI. The superiority of MR-DSWI2 was exhibited in the early detection of infestations. For example, at 5 and 10 weeks of infestation from the first swarming, MR-DSWI2 detected 15% and 90% of infested trees, while NDRE2 detected 8% and 82% of infested trees. After 12 weeks of infestation from the second swarming, the detection rates by MR-DSWI2 and NDRE2 were 67% and 57%, respectively.

3.4. Detectability of infestations

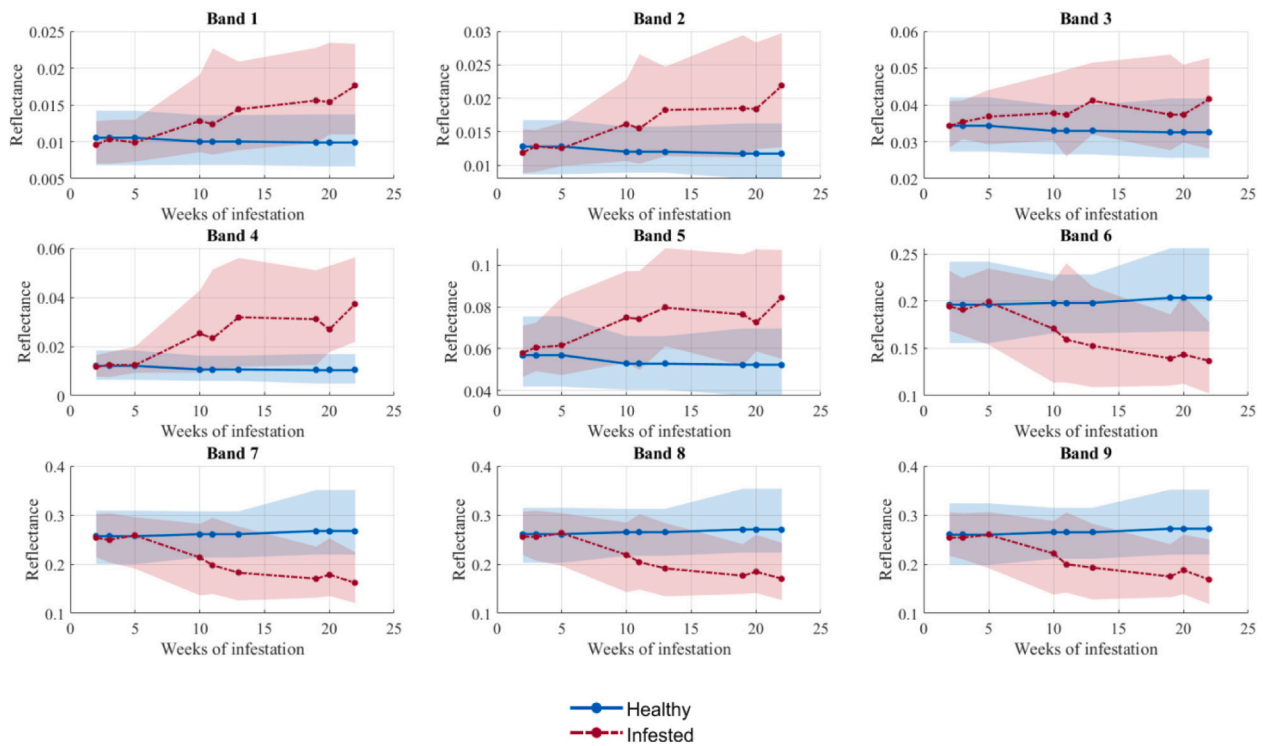
The detectability of infestations during the first swarming presented as:

During 1–5 weeks of infestation, only 15% of trees showed significantly different spectra in the drone images, and no discoloration was observed in the field. During 6–9 weeks of infestation, trees observed in the field with discoloration increased from 0 to 34%, but unfortunately we did not acquire any remote-sensing data during this stage of the study. During 10–15 weeks of infestation, 87% to 94% of trees showed significantly different spectra, while discoloration of only 48% to 74% of trees was observed in the field. Remote-sensing acquisitions stopped at 22 weeks of infestation, when all infested trees showed significantly different spectra from healthy trees, while field observations lasted for 23 weeks, by which time 90% of the trees displayed discoloration.

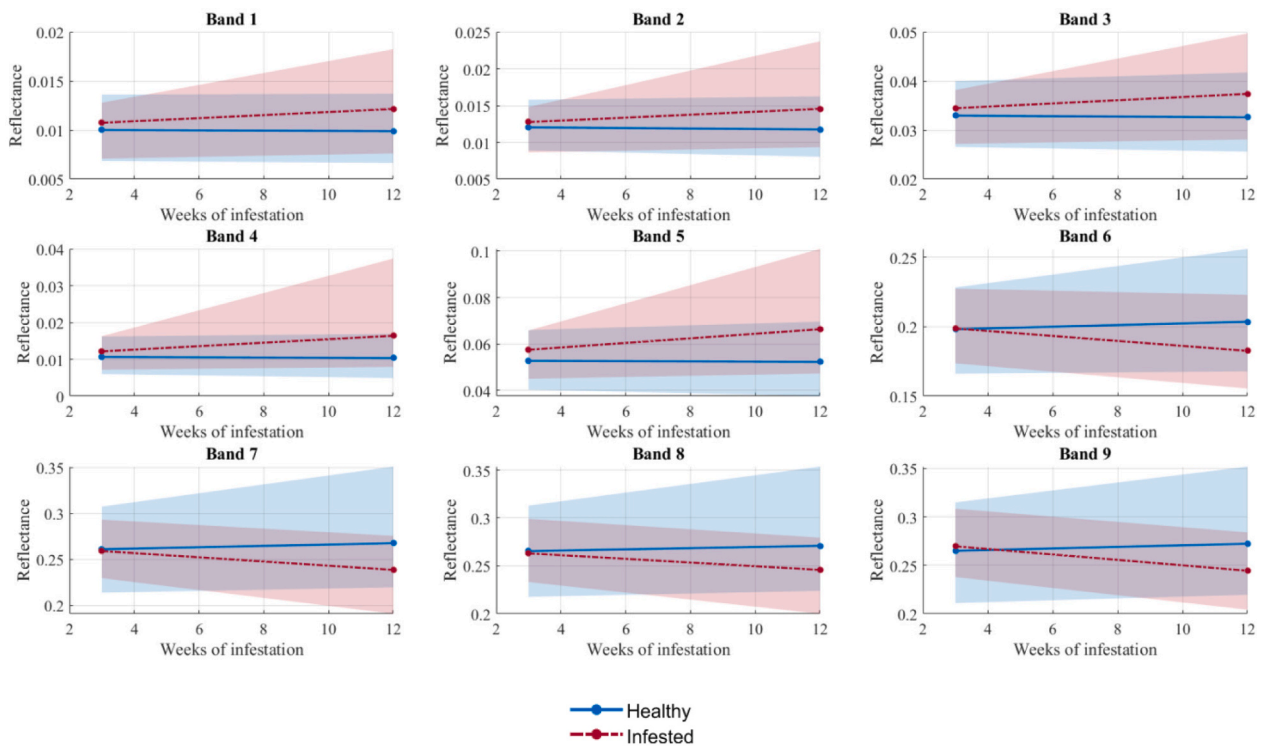
The detectability of infestations during the second swarming developed as:

During 1–6 weeks of infestation, 14% of the trees showed significantly different spectra, while no trees showed visible discoloration in the field. After 12 weeks of infestation, 67% of trees showed significantly different spectra, while 44% showed visible discoloration in the field.

Fig. 12 illustrates two extreme cases: (a) trees that had been infested



(a)



(b)

Fig. 9. Spectral changes for each band (median shown as a solid line, with 5th and 95th percentiles as bands) as infestation progressed during the first (a) and second (b) swarming.

Table 4

The separability of band reflectance of healthy and attacked trees. Light blue indicates significant differences at the $p < 0.01$ level, and dark blue indicates significant differences at the $p < 0.001$ level. The numbers in the table are the separability of the band reflectance of healthy and infested trees by LDA and larger numbers indicate larger separability.

Band No.	Band name	Infestation duration (weeks)														
		All infestations			June			August			October					
		May	June	August	October	2	3	5	3	10	11	13	12	19	20	21
1	Violet	0	0	0.4	0.5	0	0	0	0	0.4	0.3	0.5	0	0.5	0.5	0.7
2	Blue	0	0	0.4	0.6	0	0	0	0	0.3	0.5	0.6	0.2	0.5	0.5	0.6
3	Green	0	0	0.3	0.3	0	0	0	0	0.1	0.2	0.3	0.0	0.1	0.2	0.4
4	Red	0	0	0.6	0.7	0	0	0	0	0.7	0.7	0.8	0.3	0.8	0.9	0.9
5	Red-edge1	0	0	0.6	0.5	0	0	0	0	0.7	0.6	0.7	0.3	0.5	0.4	0.7
6	Red-edge2	0	0	0.5	0.7	0	0	0	0	0.3	0.4	0.5	0	0.7	0.7	0.8
7	NIR 1	0	0	0.5	0.7	0	0	0	0	0.4	0.5	0.6	0	0.8	0.7	0.8
8	NIR 2	0	0	0.5	0.7	0	0	0	0	0.4	0.5	0.6	0	0.7	0.6	0.8
9	NIR 3	0	0	0.5	0.7	0	0	0	0	0.3	0.5	0.5	0	0.6	0.6	0.7

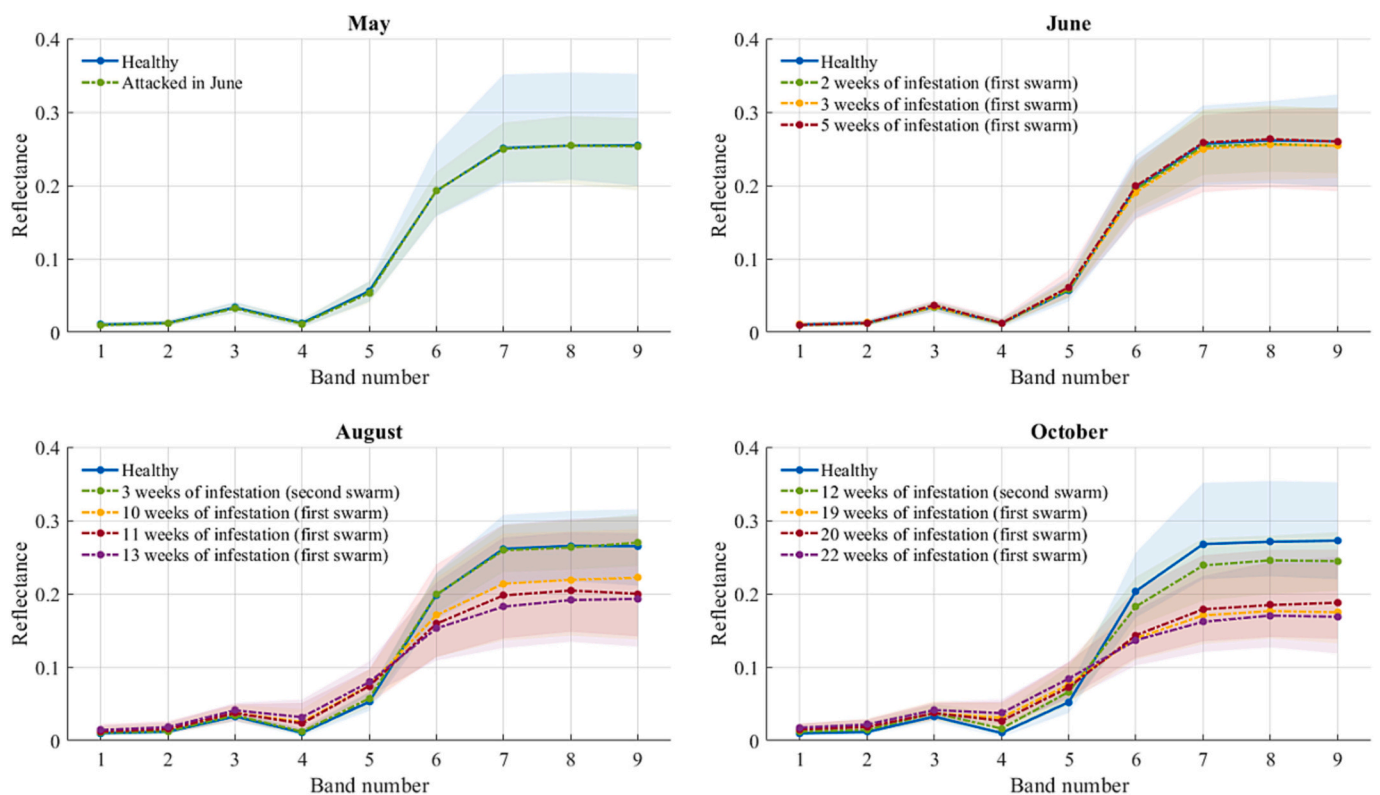


Fig. 10. The spectral signatures (median with 5th and 95th percentiles) of trees at different weeks of infestation.

for >10 weeks without showing abnormal spectra, and (b) trees showing abnormal spectra during the first 5 weeks of infestation.

4. Discussion

4.1. Spectral characteristics of infestations

The red-edge1 (band 5, 705 nm wavelength) was the first to respond to an infestation, and the only band to show significantly different

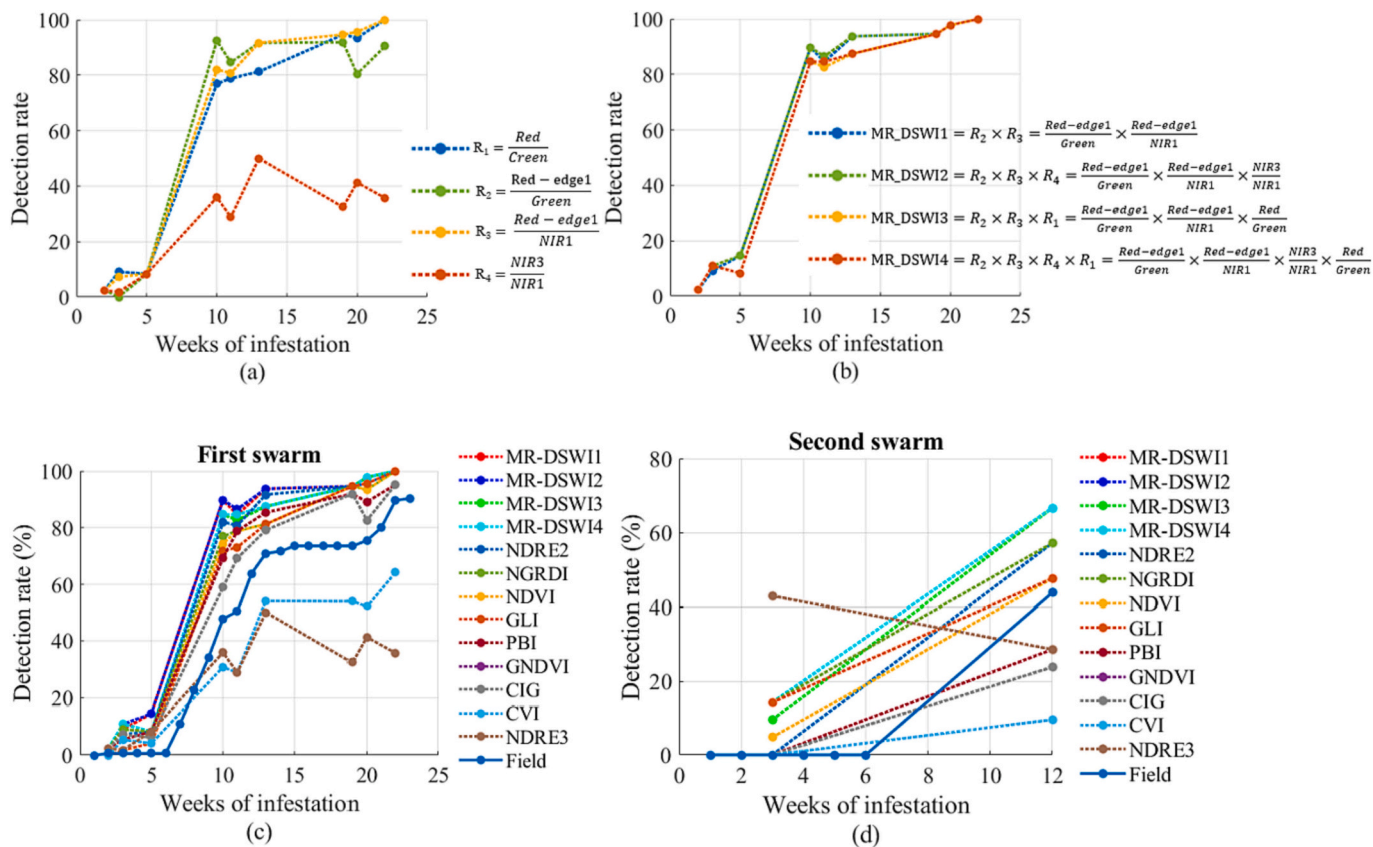


Fig. 11. Detection rates using simple ratio VIs (a) and multiple ratio VIs (b) for attacks during the first swarming, and a comparison with other VIs for trees attacked during the first (c) and second (d) swarming.

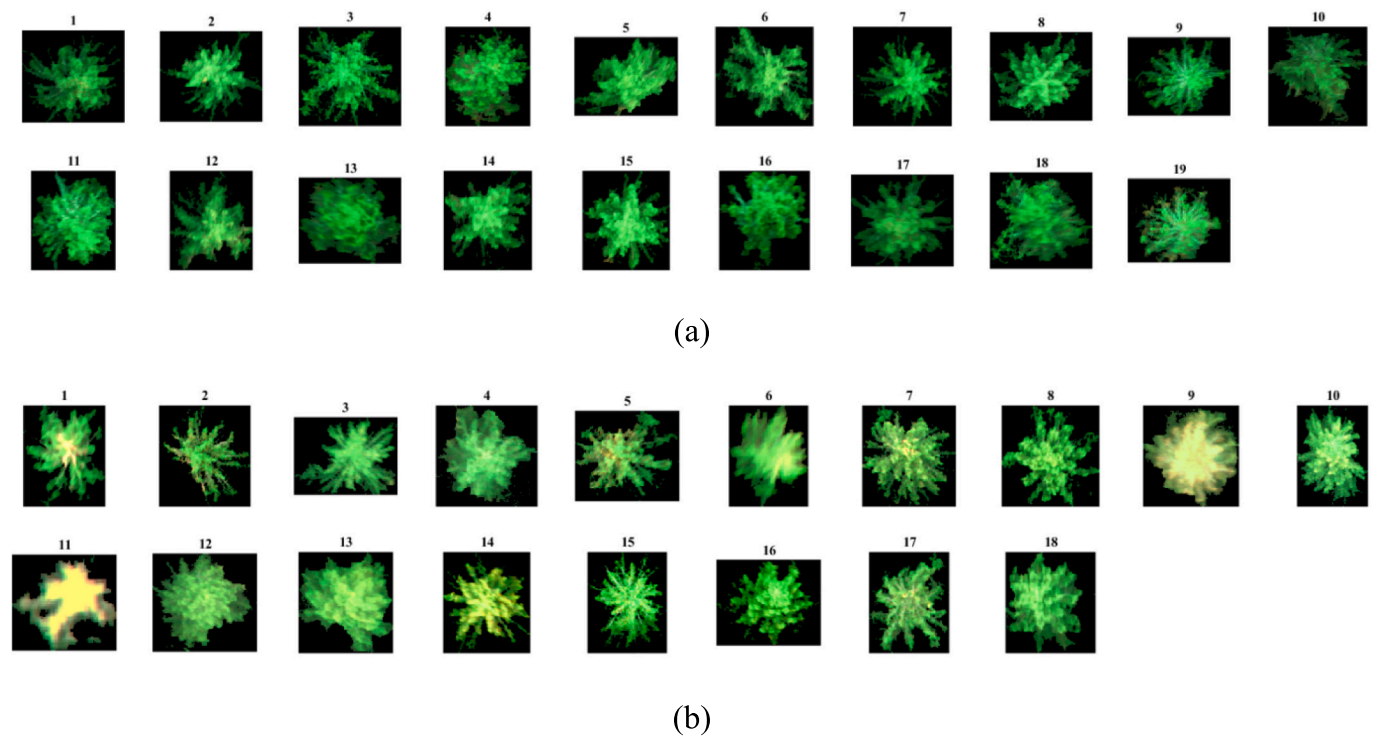


Fig. 12. (a) Trees with normal MR-DSWI2 values after >10 weeks of infestation. (b) Trees with abnormal MR-DSWI2 values after <5 weeks of infestation.

reflectance after 3 weeks of infestation. This was followed by the green band (band 3, 560 nm wavelength), which showed significantly different reflectance after 5 weeks of infestation. These two bands were the only ones that showed significantly different reflectance in the June images, but the differences were not big enough to discriminate between healthy and infested trees. The two bands were sensitive to early-stage infestations, but the separability of healthy and infested trees only increased slightly during the middle to later stages of infestation. In contrast, the second red-edge band (band 6, 740 nm) and the NIR bands were not sensitive to early stages of infestation but showed high separability at later stages of infestation. The red band (band 4, 665 nm wavelength) was the only one that showed high separability at both middle and later stages of infestation.

Almost all studies using spectral images to detect infestation have reported increased reflectance in visible bands, decreased reflectance in NIR bands, and decreased spectral derivatives in red-edge bands (i.e., a change in reflectance with respect to wavelength) (Bárta et al., 2022; Einzmann et al., 2021; Hellwig et al., 2021; Honkavaara et al., 2020; Junttila et al., 2022; Klouček et al., 2019; Cessna et al., 2021). Similar spectral responses have also been observed in trees attacked by other insects and diseases, such as the pine shoot beetle (Lin et al., 2019) and pine wilt disease (Yu et al., 2021; Iordache et al., 2020). Existing VIs usually combine two bands by presenting a ratio or normalized difference, while we proposed four disease–water stress indices using multiple ratios. Since decreasing water content, loss of chlorophyll, and structural changes in spongy mesophyll occur during different stages of infestation, the multiplication of single ratios increases the differences between healthy and infested trees and thus increases their separability. This makes our proposed method more generic and robust across all infestation stages.

The MAIA camera used in this study captured the same bands as provided in Sentinel-2 images, from the violet to NIR bands, so the spectral responses of corresponding bands from the different sensor platforms could be compared. When infested trees lost their vitality, the reflectance of the blue to red-edge1 bands in the drone images increased, and similar changes were observed in Sentinel-2 data (Huo et al., 2021; Bárta et al., 2021; Abdullah et al., 2019b). The reflectance of the red-edge2 and the NIR bands decreased in the drone images after infestation. In Huo et al. (2021), the reflectance of these bands in attacked trees was higher than in healthy trees before the attacks, and lasted until later stages of infestation. In Bárta et al. (2021), both increased and decreased reflectance of these bands were observed at different infestation stages because of the influence of the canopy structure. Inconsistent changes in NIR bands have also been seen in other studies using different sensors and platforms (Ortiz et al., 2013; Klouček et al., 2019), possibly because the NIR bands are responding to factors other than insect infestation. The two red-edge bands responded to early infested trees in Bárta et al. (2021) when using Sentinel-2, but neither of them responded in Huo et al. (2021). In this study, only the red-edge1, and not red-edge2, responded in the drone images. More studies are needed to investigate the factors influencing the response of red-edge bands.

4.2. Temporal characteristics of infestations

4.2.1. Whether it is possible to detect infestations in June

In 2021, the first bark beetle swarming in the study area started in week 20 (May 17). No sampled trees had been infested from previous years, and no spectral differences were observed before the attack between healthy trees and trees that were later attacked. Five weeks after the beginning of the attacks, i.e., in late June, infested trees did not show discoloration in the field (green attack) but did show significant increasing reflectance in the green band (band 4) and red-edge band (band 5). It could be that the multispectral images captured differences between healthy and green-attack trees, but it should be borne in mind that 91% of the green-attack trees still had spectra within the range of the healthy trees in June. Therefore, based on the environmental

conditions of our study, we do not think early detection of infestations is feasible in June (1 month after a swarming). This is in agreement with a previous study (Huo et al., 2021) in the same area, in which spectral differences between healthy and attacked trees existed in Sentinel-2 images taken before the attacks, and these differences did not increase during May and June (1 and 2 months after a swarming).

In central Europe, swarming happens earlier, more often and more intensely than in northern Europe, explaining why some studies have shown detectability in June. One study observed swarming in April, May, and August, and could separate healthy and attacked trees in a Sentinel-2 image at the end of May (Bárta et al., 2021). In another study (Bárta et al., 2022), spectral differences between healthy and attacked trees existed before attacks, and were not significant enough to identify infested trees in May and June, but were significant enough in July (2 months after the swarming and 1 month after infestation). Some studies have observed spectral differences between healthy and attacked trees in June but did not test whether the spectral differences existed before the attacks (Abdullah et al., 2019b, 2019c).

4.2.2. Whether and when it is possible to detect green attacks

This study presents clear evidence that spectral data can reveal infestations before crown discoloration, i.e. we were able to detect green attacks. Although the same conclusion has been drawn in many studies based on spectral differences between healthy and green-attack trees (Honkavaara et al., 2020; Minařík et al., 2021), our study has specifically demonstrated that the spectral differences were caused by infestations because no significant spectral differences existed before the attacks. The detection rates from multispectral images were consistently higher than those detected by discoloration in the field. During the first swarming, we identified 90% of the infested trees after 10 weeks of infestation using multispectral images, about twice the number of trees detected in the field based on discoloration. We conclude that infested trees can be detected earlier using multispectral images than field observations based on crown colors.

Vitality decay caused by infestations takes place on a continuum. Therefore, instead of dividing infestations into separate stages, e.g., green, yellow, and red attacks, we grouped trees according to the number of weeks of infestation, and plotted a continuous curve of infestation detectability over time. There were large variances between individual trees regarding the infestation stage, e.g., some trees were still in the green-attack phase after 10 weeks of infestation, while other trees were in the yellow-attack phase after just 5 weeks of infestation. We assume this is related to variability in tree vulnerability. By quantifying the detectability, instead of qualitatively describing detectable green attacks, we were able to consider the variation between individual trees.

During the first swarming, 15% of the infested trees were identified after 5 weeks of infestation, and 90% were identified after 10 weeks. We had intended to analyze the spectral responses during July, but were unable to acquire images during this period because of drone damage. This created a gap in the time series of images for trees at 6–9 weeks of infestation. The field observations showed a linear increase in the number of discolored trees during weeks 6–13 of infestation. Both the spectral changes in the images and discoloration observed in the field are indicators of vitality loss, hence we assume that there would be a period when the detectability of infested trees from multispectral images increases in a similar manner. However, we could not determine this period more precisely than 5–10 weeks of infestation, and we cannot reject the possibility that this period might be shorter than 10 weeks, e.g., 6–9 weeks of infestation. During this period of rapid change, it is essential that we can determine how early infestations can be detected. Taking all the different VIs into consideration, we did not see any indication that infested trees can be detected sufficiently during the first 5 weeks of infestation, but most infested trees can be detected after 10–13 weeks of infestation.

Although the detection rates differed between different VIs, they did

not change the overall conclusion of how early infestations could be detected. The newly proposed MR-DSWI2 and MR-DSWI3 detected 15% of the attacked trees at 5 weeks of infestation, while other VIs detected 5–8% of the trees. The newly proposed MR-DSWIs and NDRE2 detected >80% of the trees at 10 weeks of infestation, while the other VIs, apart from CVI and NDRE3, indicated similar detection rates at 13 weeks of infestation.

One goal of developing early detection techniques is to enable the identification and removal of infested trees when the larvae are still inside the bark, on the assumption that this will reduce the size of a second swarming and the number of attacked trees. Attacks from the second swarming (week 30) were observed 10 weeks after the first attacks (week 20) in this study. In practice, 6–9 weeks after an attack begins is likely to be the most efficient period for detecting and removing infested trees (which would be around July for the study area). Classifying trees too early during the infestation period would result in insufficient detection rates, while too late would result in less time for sanitation felling and an increased risk of a second swarming arising from individual variations.

4.2.3. Factors influencing the critical period for detecting green attacks

In our field experiment, 75% of the trees were attacked before week 25 (June 21–27), and 10% were attacked in week 30 (July 26 to August 1). We assumed that these two attacks originated from the first and second swarming, respectively. After 11 weeks of infestation by the first swarming, 85% of the trees were detected, while the detection rate during the second swarming was only 67% after 12 weeks of infestation. Different factors may cause this phenomenon, e.g., the attacks from the second swarming may have been less intense, or the trees attacked in late summer might have been less vulnerable compared with those attacked in the spring and early summer. Both of these factors would result in more trees defending themselves successfully or losing vitality more slowly after the second swarming. Temperature is a crucial factor in the intensity of attacks, and water-related stress influences the general vulnerability of spruces. In this study, we only exhibit temperature data in Fig. 2 for potential reference to other studies, but it was not further analyzed. More research is needed on how much these two factors influence the temporal characteristics of infestation development. A study in southern Czech Republic (Bárta et al., 2022) recorded attacks starting in week 19 (May 3, 2020) in recent forest edges, and identified infestations of trees in the monitored area in week 24 (June 17) by the field inventory. Four weeks later (in week 28, July 10), the 25th and 75th percentile of spectra from healthy and attacked individual trees showed significant differences in the hyperspectral images. The recommended period in the Czech Republic for removing infested trees is within 6 weeks of infestation, i.e. the developmental time from egg to imago (Bárta et al., 2022). The critical period for detecting green attacks may therefore be about 4–6 weeks in central Europe and about 5–9 weeks in Scandinavia, based on this limited number of studies. The attacks in central Europe may have been more intense than those in Sweden, causing the attacked trees to lose vitality faster, because of the warmer temperature zone. Another study in central Czech Republic observed three swarming in 2018, around mid-April, late May, and early August. The attacked tree groups started to show separable spectra in Sentinel-2 images on May 31. We assume that satellite images capture subtle changes later than drone images because of their lower spatial resolution, but more studies are needed to verify these assumptions.

4.3. Application potential, limitations, and further studies

We conducted weekly field observations and considered infestations to have started when we observed entrance holes in the bark. Because entrance holes further up on the stems are not as easy to observe, the attacks may have started earlier than presented here. Nevertheless, the swarming monitoring using the flight intercept traps also indicated the start of the attacks and decreased the probability of delayed observation.

Because of limitations with the drone flights, we did not obtain any drone images for weeks 6–9 of infestation during the first swarming, which should be a focus for future studies. The second swarming was less intense compared with the first, and we only observed 21 attacked trees. Therefore, the temporal-spectral analysis of the infestations from the second swarming is limited. This study mainly focused on trees attacked in the first swarming, and only monitored the second swarming until the green-attack stage. From the October drone image, 67% of the infested trees were detected, and damage control could be conducted. Exploring whether the remaining 33% of infested trees could be detected before the first swarming in the following year would be an interesting topic to pursue, and could contribute to population control planning. Future studies should also explore the potential of using hyperspectral images, which could provide slightly better detection rates compared with multispectral imagery (Honkavaara et al., 2020). Hyperspectral images would enable research on whether continuous spectral curves can provide more information for earlier detection than multispectral images. Many studies using satellite images have proposed SWIR bands for early detection from June to August (Immitzer and Atzberger, 2014; Huo et al., 2021), and so have spectrometer studies of needle reflectance (Abdullah et al., 2018; Reichmuth et al., 2018; Einzmann et al., 2021). In this study, we could not assess whether the SWIR bands were useful or not, but we encourage further research on the potential use of high-resolution SWIR bands for the early detection of infestations, by mounting SWIR sensors on drones.

How early the infested trees show abnormal spectra should be answered both from the perspective of remote-sensing techniques and the colonization process and its drivers. We have presented spectra separability for infestations at different stages, and proposed new VIs that achieved higher detection rates for green attacks compared with existing VIs. Our proposed methodology could be a useful tool for quantifying vitality loss and supporting research on host-tree vulnerability, the colonization process, and driving factors. For example, in this study, 9% of infested trees showed abnormal spectra during weeks 1–5 of infestation (i.e., vulnerable trees were identified), and 6% of the infested trees did not show abnormal spectra after 13 weeks of infestation (i.e., invulnerable trees were identified). Mapping the occurrence of infestations and the vulnerabilities of trees could contribute to modeling environmental factors and estimating attack risk.

For forest monitoring, drone image acquisition is more flexible in time and area compared to satellite images, and with higher spatial resolution providing health stages at the individual-tree level. The coverage of drone images is not sufficient for wall-to-wall mapping of large areas, nevertheless, this study provides valuable insights for large-area mapping. First, the study shows that it appears almost impossible to detect green attacks in June in Sweden, saving lots of effort attempting to use satellite images to detect infestations before July. It also indicates massive false positive detections in the large-area mapping if satellite images before July are used, since the abnormal spectrum is unlikely from the green attacks. Second, the proposed framework of early detection using drone images is suitable for the focused monitoring of small areas, and it is faster and more accurate than field inventory, thus can provide ground-truth data for large-area mapping.

5. Conclusions

We conducted weekly field observations on spruces attacked by bark beetles, and acquired and analyzed multispectral drone images before and during different stages of infestation. The red-edge band with a 705 nm wavelength was the first band to respond to infestations, followed by the green band (with a 560 nm wavelength). We have developed new disease–water stress indices (MR-DSWIs) by multiplying ratios of green, red, red-edge, and NIR bands. Using these MR-DSWIs resulted in higher detection rates of infestations than previously used VIs: during the first swarming, 15% of infested trees were detected after 5 weeks of infestation, and 90% were detected after 10 weeks. We conclude that, during

the first swarming, weeks 5–10 of infestation represent a key period for detection. The detection rates from multispectral images were higher than the rates of discoloration observed in the field throughout the whole season. Thus, we conclude that green attacks are detectable from multispectral drone images, and the proposed methods could be used for mapping local infestations at an early stage and indicating tree vitality.

This study has addressed the question of how early trees infested by bark beetles show significantly different spectra compared with healthy trees. We encourage further studies that replicate and extend our results, with longer monitoring periods, including second and/or third swarming, spanning more years, and encompassing more climate zones.

CRediT authorship contribution statement

Langning Huo: Conceptualization, Methodology, Software, Validation, Formal analysis, Investigation, Resources, Data curation, Writing – original draft, Writing – review & editing, Visualization, Supervision, Project administration, Funding acquisition. **Eva Lindberg:** Conceptualization, Methodology, Writing – original draft, Writing – review & editing, Funding acquisition. **Jonas Bohlin:** Methodology, Data curation, Writing – review & editing. **Henrik Jan Persson:** Conceptualization, Methodology, Validation, Formal analysis, Investigation, Writing –

original draft, Writing – review & editing, Funding acquisition.

Declaration of Competing Interest

The authors declare that they have no known competing financial interests or personal relationships that could have appeared to influence the work reported in this paper.

Data availability

The authors do not have permission to share data.

Acknowledgments

This project was funded by Hildur & Sven Wingquist's Foundation for Forest Science Research, the SLU Forest Damage Center, the Stiftelsen Seydlitz MP bolagen Foundation, and the Stiftelsen Nils och Dorthi Troëdssons Foundation. We thank Ronja Risberg for conducting the weekly field observations. We acknowledge Ronja Risberg, Giovanni D'Amico, Emanuele Papucci, Mats Söderström, Jörgen Wallerman, Johan Fransson, Niwen Li, and Yining Lian for their help during the drone flights.

Appendix A. Swarming monitoring

Three types of swarming monitoring were used as shown in Fig. A.

(1) Swarming monitored by the Swedish Forest Agency (SFA). The SFA organizes the swarming monitoring in 64 locations throughout Sweden. Big traps with pheromone bags were mounted in clear-cut areas surrounded by spruce forests. The traps were emptied every Monday and the number of trapped beetles was published every week. The closest trap to our study area was about 9 km away, and the number of trapped beetles is illustrated in Fig. A with blue bars. (<https://www.skogsstyrelsen.se/statistik/statistik-efter-amne/svarmningsovervakning/>)

(2) In this study, we used a trap from the SFA and put it in a clear-cut area within the study area. The number of trapped beetles is illustrated in Fig. A with red bars.

(3) In this study, we attached a flight interception trap (Ranius and Jansson, 2002) on each central tree in every attacked plot to monitor the swarming. The traps were made from a flat, vertical piece of transparent plastic with a container below with a mix of glycol (we used windshield washer fluid), water, and detergent to lower the surface tension (Fig. 1d). We counted bark beetles every week from week 16 (April 5) to week 28 (July 12). The number of beetles is illustrated in Fig. A with yellow bars.

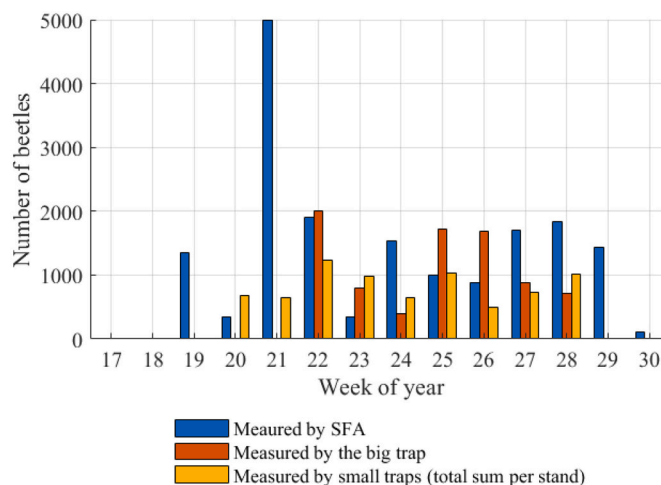


Fig. A. The number of beetles monitored by (1) the SFA (blue bars), in this study using (2) a big trap (red bars), and (3) small traps (yellow bars). (For interpretation of the references to colour in this figure legend, the reader is referred to the web version of this article.)

Appendix B. The DBH distribution of the sample trees

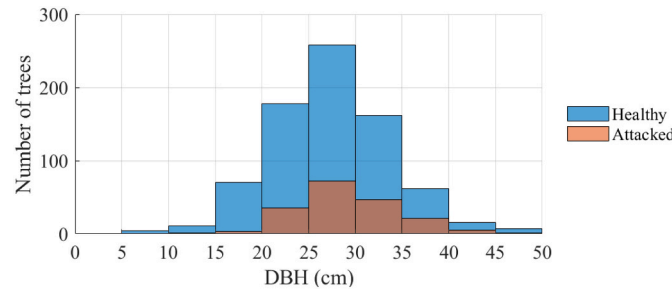


Fig. B. The DBH distribution of healthy and attacked trees.

Appendix C. Sensitivity analysis (% detection rate) for T_{hgreen} values using MR-DSWI2.

T_{hgreen}	Weeks of infestation										
	First swarming									Second swarming	
	2	3	5	10	11	13	19	20	22	3	12
0	0	5	13	90	83	92	92	89	93	10	71
0.005	0	5	13	90	83	92	92	89	93	10	67
0.01	5	7	15	90	87	94	95	96	98	10	62
0.015	2	11	15	90	87	94	95	98	100	10	67
0.02	2	11	15	87	83	94	95	98	100	10	67
0.025	2	11	15	85	83	94	95	96	100	5	62
0.03	5	11	15	85	83	94	95	96	100	5	62

Appendix D. Detection rate (%) of infested trees based on different VIs.

VI	Weeks of infestation										
	First swarming									Second swarming	
	2	3	5	10	11	13	19	20	22	3	12
MR-DSWI1	2	9	15	90	85	94	95	98	100	10	67
MR-DSWI2	2	11	15	90	87	94	95	98	100	10	67
MR-DSWI3	2	11	8	85	83	88	95	98	100	10	67
MR-DSWI4	2	11	8	85	85	88	95	98	100	14	67
NDRE2	2	7	8	82	81	92	95	96	100	0	57
NGRDI	2	9	8	77	79	81	95	93	100	14	57
NDVI	0	7	6	74	79	81	95	93	100	5	48
GLI	0	2	4	72	73	81	95	96	100	14	48
PBI	2	5	8	69	79	85	92	89	95	0	29
GNDVI	2	7	6	59	69	79	92	83	95	0	24
CIG	2	7	6	59	69	79	92	83	95	0	24
CVI	0	5	4	31	29	54	54	52	64	0	10
NDRE3	2	2	8	36	29	50	32	41	36	43	29

References

Abdullah, Haidi, Darvishzadeh, Roshanak, Skidmore Andrew, K., Groen Thomas, A., Heurich, Marco, 2018. European spruce bark beetle (*Ips typographus*, L.) green attack affects foliar reflectance and biochemical properties. *Int. J. Appl. Earth Obs. Geoinf* 64, 199–209. <https://doi.org/10.1016/j.jag.2017.09.009>.

Abdullah, H., Darvishzadeh, R., Skidmore, A., Heurich, M., 2019a. Sensitivity of Landsat-8 OLI and TIRS data to foliar properties of early stage bark beetle (*Ips typographus*L.) infestation. *Remote Sens.* 11, 398.

Abdullah, H., Skidmore, A.K., Darvishzadeh, R., Heurich, M., 2019b. Sentinel-2 accurately maps green-attack stage of European spruce bark beetle (*Ips typographus* L.) compared with Landsat-8. *Remote Sens. Ecol.Conserv.* 5, 87–106.

Abdullah, H., Skidmore, A.K., Darvishzadeh, R., Heurich, M., 2019c. Timing of red-edge and shortwave infrared reflectance critical for early stress detection induced by bark beetle (*Ips typographus*, L.) attack. *Int. J. Appl. Earth Obs. Geoinf.* 82, 101900.

Annala, E., 1969. Influence of temperature upon the development and voltinism of *Ips typographus* L. (Coleoptera, Scolytidae). *Annales Zoologici Fennici* 6. <http://www.jstor.org/stable/23731366>.

Atzberger, C., Zeug, G., Defourny, P., Aragão, L., Hammarström, L., Immitzer, M., 2020. Monitoring of forests through remote sensing : final report. Publications Office.

Barnes, E.M., Clarke, T.R., Richards, S.E., Colaizzi, P.D., Haberland, J., Kostrzewski, M., Waller, P., Choi, C., Riley, E., Thompson, T., Lascano, R.J., Li, H., Moran, M.S. (Eds.), 2000. Coincident Detection of Crop Water Stress, Nitrogen Status, and Canopy Density Using Ground-Based Multispectral Data.

Bárta, V., Hanuš, J., Dobrovolný, L., Homolová, L., 2022. Comparison of field survey and remote sensing techniques for detection of bark beetle-infested trees. *For. Ecol. Manag.* 506, 119984.

Bárta, V., Lukeš, P., Homolová, L., 2021. Early detection of bark beetle infestation in Norway spruce forests of Central Europe using Sentinel-2. *Int. J. Appl. Earth Obs. Geoinf.* 100, 102335.

Cessna, J., Alonzo, M.G., Foster, A.C., Cook, B.D., 2021. Mapping boreal forest spruce beetle health status at the individual crown scale using fused spectral and structural data. *Forests* 12, 1145.

Christiansen, E., Bakke, A., 1988. The spruce bark beetle of Eurasia. In: Berryman, A.A. (Ed.), *Dynamics of Forest Insect Populations: Patterns, Causes, Implications*. Springer, US, Boston, MA, pp. 479–503.

- Coops, N.C., Johnson, M., Wulder, M.A., White, J.C., 2006a. Assessment of QuickBird high spatial resolution imagery to detect red attack damage due to mountain pine beetle infestation. *Remote Sens. Environ.* 103, 67–80.
- Coops, N.C., Shang, C., Wulder, M.A., White, J.C., Hermosilla, T., 2020. Change in forest condition: characterizing non-stand replacing disturbances using time series satellite imagery. *For. Ecol. Manag.* 474, 118370.
- Coops, N.C., Wulder, M.A., White, J.C., 2006b. Integrating remotely sensed and ancillary data sources to characterize a mountain pine beetle infestation. *Remote Sens. Environ.* 105, 83–97.
- Ehammer, A., Fritsch, S., Conrad, C., Lamers, J., Dech, S., 2010. Statistical derivation of fPAR and LAI for irrigated cotton and rice in arid Uzbekistan by combining multi-temporal RapidEye data and ground measurements. In: Neale, C.M.U., Maltese, A. (Eds.), *Remote Sensing for Agriculture, Ecosystems, and Hydrology XII*. SPIE, p. 782409.
- Einzmann, K., Atzberger, C., Pinnel, N., Glas, C., Böck, S., Seitz, R., Immitzer, M., 2021. Early detection of spruce vitality loss with hyperspectral data: results of an experimental study in Bavaria, Germany. *Remote Sens. Environ.* 266, 112676.
- Fang, S., Cui, R., Wang, Y., Zhao, Y., Yu, K., Jiang, A., 2021. Application of multiple spectral systems for the tree disease detection: a review. *Appl. Spectrosc. Rev.* 68, 1–27.
- Fassnacht, F.E., Latifi, H., Ghosh, A., Joshi, P.K., Koch, B., 2014. Assessing the potential of hyperspectral imagery to map bark beetle-induced tree mortality. *Remote Sens. Environ.* 140, 533–548.
- Foster, A.C., Walter, J.A., Shugart, H.H., Sibold, J., Negron, J., 2017. Spectral evidence of early-stage spruce beetle infestation in engelmann spruce. *For. Ecol. Manag.* 384, 347–357.
- Gamon, J.A., Serrano, L., Surfus, J.S., 1997. The photochemical reflectance index: an optical indicator of photosynthetic radiation use efficiency across species, functional types, and nutrient levels. *Oecologia* 112, 492–501.
- Gitelson, A.A., Gritz, Y., Merzlyak, M.N., 2003. Relationships between leaf chlorophyll content and spectral reflectance and algorithms for non-destructive chlorophyll assessment in higher plant leaves. *J. Plant Physiol.* 160, 271–282.
- Gitelson, A.A., Merzlyak, M.N., 1998. Remote sensing of chlorophyll concentration in higher plant leaves. *Adv. Space Res.* 22, 689–692.
- Hellwig, F.M., Stelmaszczyk-Górska, M.A., Dubois, C., Wolsza, M., Truckenbrodt, S.C., Sagichewski, H., Chmara, S., Bannehr, L., Lausch, A., Schmuilius, C., 2021. Mapping European spruce bark beetle infestation at its early phase using gyrocopter-mounted hyperspectral data and field measurements. *Remote Sens.* 13, 4659.
- Hermosilla, T., Wulder, M.A., White, J.C., Coops, N.C., 2019. Prevalence of multiple forest disturbances and impact on vegetation regrowth from interannual landsat time series (1985–2015). *Remote Sens. Environ.* 233, 111403.
- Hlásný, T., Zimová, S., Merganičová, K., Štěpánek, P., Modlinger, R., Turčáni, M., 2021. Devastating outbreak of bark beetles in the Czech Republic: drivers, impacts, and management implications. *For. Ecol. Manag.* 490, 119075.
- Honkavaara, E., Näsi, R., Oliveira, R., Viljanen, N., Suomalainen, J., Khoramshahi, E., Hakala, T., Nevalainen, O., Markelin, L., Vuorinen, M., Kankaanhuhta, V., Lyytikäinen-Saarenmaa, P., Haataja, L., 2020. In: *Using Multitemporal Hyper- and Multispectral UAV Imaging For Detecting Bark Beetle Infestation on Norway Spruce*. The International Archives of the Photogrammetry, Remote Sensing and Spatial Information Sciences, XLIII-B3-2020, pp. 429–434.
- Hunt, E.R., Daughtry, C.S.T., Eitel, J.U.H., Long, D.S., 2011. Remote sensing leaf chlorophyll content using a visible band index. *Agron. J.* 103, 1090–1099.
- Huo, L., Lindberg, E., Fransson, J.E.S., Persson, H.J., 2022. Comparing spectral differences between healthy and early infested spruce forests caused by bark beetle attacks using satellite images. In: *IGARSS 2022 - 2022 IEEE International Geoscience and Remote Sensing Symposium*, pp. 7709–7712.
- Huo, L., Persson, H.J., Lindberg, E., 2021. Early detection of forest stress from European spruce bark beetle attack, and a new vegetation index: normalized distance red & SWIR (NDRS). *Remote Sens. Environ.* 255, 112240.
- Immitzer, M., Atzberger, C., 2014. Early Detection of Bark Beetle Infestation in Norway Spruce (*Picea abies*, L.) using WorldView-2 Data. *Photogrammetrie - Fernerkundung - Geoinformation* 2014, 351–367.
- Iordache, M.-D., Mantas, V., Baltazar, E., Pauly, K., Lewyckij, N., 2020. A machine learning approach to detecting pine wilt disease using airborne spectral imagery. *Remote Sens.* 12, 2280.
- Junttila, S., Näsi, R., Koivumäki, N., Imangholilo, M., Saarinen, N., Raisio, J., Holopainen, M., Hyypä, H., Hyypä, J., Lyytikäinen-Saarenmaa, P., Vastaranta, M., Honkavaara, E., 2022. Multispectral. *Remote Sens.* 14, 909.
- Klouček, T., Komárek, J., Surový, P., Hrach, K., Janata, P., Vašíček, B., 2019. The use of UAV mounted sensors for precise detection of bark beetle infestation. *Remote Sens.* 11, 1561.
- Latifi, H., Schumann, B., Kautz, M., Dech, S., 2014. Spatial characterization of bark beetle infestations by a multivariate synergy of SPOT and Landsat imagery. *Environ. Monit. Assess.* 186, 441–456.
- Lausch, A., Heurich, M., Gordalla, D., Dobner, H.-J., Gwilym-Margianto, S., Salbach, C., 2013. Forecasting potential bark beetle outbreaks based on spruce forest vitality using hyperspectral remote-sensing techniques at different scales. *For. Ecol. Manag.* 308, 76–89.
- Li, M., Li, H., Ding, X., Wang, L., Wang, X., Chen, F., 2022a. The detection of pine wilt disease: a literature review. *Int. J. Mol. Sci.* 23.
- Li, N., Huo, L., Zhang, X., 2022b. Classification of pine wilt disease at different infection stages by diagnostic hyperspectral bands. *Ecol. Indic.* 142, 109198.
- Li, N., Zhang, X., Huo, L., 2022. Identifying nematode-induced wilt using hyperspectral drone images and assessing the potential of early detection. In: *IGARSS 2022 - 2022 IEEE International Geoscience and Remote Sensing Symposium*, pp. 512–515.
- Lin, Q., Huang, H., Wang, J., Huang, K., Liu, Y., 2019. Detection of Pine Shoot Beetle (PSB) stress on pine forests at individual tree level using UAV-based hyperspectral imagery and Lidar. *Remote Sens.* 11, 2540.
- Louhaichi, M., Borman, M.M., Johnson, D.E., 2001. Spatially located platform and aerial photography for documentation of grazing impacts on wheat. *Geocarto Int.* 16, 65–70.
- Luo, Y., Huang, H., Roques, A., 2022. Early. *Annu. Rev. Entomol.* 68:277–298.
- Marvasti-Zadeh, S.M., Goodson, D., Ray, N., Erbilgin, N., 2022. Early Detection of Bark Beetle Attack Using Remote Sensing and Machine Learning: A Review.
- Meurisse, N., Coullien, D., Grégoire, J.-C., 2008. Kairomone traps: a tool for monitoring the invasive spruce bark beetle *Dendroctonus micans* (Coleoptera: Scolytinae) and its specific predator, *Rhizophagus grandis* (Coleoptera: Monotomidae). *J. Appl. Ecol.* 45, 537–548.
- Minářik, R., Langhammer, J., 2016. In: *Use of a multispectral UAV photogrammetry for detection and tracking of forest disturbance dynamics*. ISPRS - International Archives of the Photogrammetry, Remote Sensing and Spatial Information Sciences, XLI-B8, pp. 711–718.
- Minářik, R., Langhammer, J., Lendziach, T., 2020. Automatic tree crown extraction from UAS multispectral imagery for the detection of bark beetle disturbance in mixed forests. *Remote Sens.* 12, 4081.
- Minářik, R., Langhammer, J., Lendziach, T., 2021. Detection of bark beetle disturbance at tree level using UAS multispectral imagery and deep learning. *Remote Sens.* 13, 4768.
- Näsi, R., Honkavaara, E., Blomqvist, M., Lyytikäinen-Saarenmaa, P., Hakala, T., Viljanen, N., Kantola, T., Holopainen, M., 2018. Remote sensing of bark beetle damage in urban forests at individual tree level using a novel hyperspectral camera from UAV and aircraft. *Urban For. Urban Green.* 30, 72–83.
- Näsi, R., Honkavaara, E., Lyytikäinen-Saarenmaa, P., Blomqvist, M., Litkey, P., Hakala, T., Viljanen, N., Kantola, T., Tanhuanpää, T., Holopainen, M., 2015. Using UAV-based photogrammetry and hyperspectral imaging for mapping bark beetle damage at tree-level. *Remote Sens.* 7, 15467–15493.
- Navarro, G., Caballero, I., Silva, G., Parra, P.-C., Vázquez, Á., Caldeira, R., 2017. Evaluation of forest fire on Madeira Island using Sentinel-2A MSI imagery. *Int. J. Appl. Earth Obs. Geoinf.* 58, 97–106.
- Niemann, K.O., Quinn, G., Stephen, R., Visintini, F., Parton, D., 2015. Hyperspectral remote sensing of mountain pine beetle with an emphasis on previsual assessment. *Can. J. Remote Sens.* 41, 191–202.
- Öhrn, P., Långström, B., Lindelöv, Å., Björklund, N., 2014. Seasonal flight patterns of Ips typographus in southern Sweden and thermal sums required for emergence. *Agric. For. Entomol.* 16, 147–157.
- Ortiz, S., Breidenbach, J., Kändler, G., 2013. Early detection of bark beetle green attack using TerraSAR-X and RapidEye data. *Remote Sens.* 5, 1912–1931.
- Ozcan, G.E., Cicek, O., Enez, K., Yildiz, M., 2014. A new approach to determine the capture conditions of bark beetles in pheromone-baited traps. *Biotechnol. Biotechnol. Equip.* 28, 1057–1064.
- Penuelas, J., Fillella, I., Gamon, J.A., 1995. Assessment of photosynthetic radiation-use efficiency with spectral reflectance. *New Phytol.* 131, 291–296.
- Puritch, G.S., 1981. Nonvisual remote sensing of trees affected by stress—a review: Environment Canada. Canadian Forestry Service, Pacific Forest Research Centre, Victoria, BC.
- Ranius, T., Jansson, N., 2002. A comparison of three methods to survey saproxylic beetles in hollow oaks. *Biodivers. Conserv.* 11 <https://doi.org/10.1023/A:10203430300085>.
- Reichmuth, Anne, Henning, Lea, Pinnel, Nicole, Bachmann, Martin, Rogge, Derek, 2018. Early Detection of Vitality Changes of Multi-Temporal Norway Spruce Laboratory Needle Measurements—The Ring-Barking Experiment. *Remote Sensing* 10 (2), 57. <https://doi.org/10.3390/rs10010057>.
- Rouse, J., Haas, R., Schell, J., Deering, D. (Eds.), 1973. *Monitoring Vegetation Systems in the Great Plains with ERTS*.
- Schroeder, L.M., 2013. Monitoring of Ips typographus and Pityogenes chalcographus : influence of trapping site and surrounding landscape on catches. *Agric. For. Entomol.* 15, 113–119.
- Schuld, B., Buras, A., Arend, M., Vitase, Y., Beierkuhnlein, C., Damm, A., Gharun, M., Grams, T.E.E., Hauck, M., Hajek, P., Hartmann, H., Hiltbrunner, E., Hoch, G., Holloway-Phillips, M., Körner, C., Larysch, E., Lübke, T., Nelson, D.B., Rammig, A., Rigling, A., Rose, L., Rühr, N.K., Schumann, K., Weiser, F., Werner, C., Wohlgemuth, T., Zang, C.S., Kahmen, A., 2020. A first assessment of the impact of the extreme 2018 summer drought on Central European forests. *Basic Appl. Ecol.* 45, 86–103.
- Seidl, R., Schelhaas, M.-J., Rammer, W., Verker, P.J., 2014. Increasing forest disturbances in Europe and their impact on carbon storage. *Nat. Clim. Chang.* 4, 806–810.
- Senf, C., Sebald, J., Seidl, R., 2020. Increases in canopy mortality and their impact on the demographic structure of Europe's forests.
- Senf, C., Seidl, R., Hostert, P., 2017. Remote sensing of forest insect disturbances: current state and future directions. *Int. J. Appl. Earth Observ. Geoinform. ITC J.* 60, 49–60.
- Tanase, M.A., Aponte, C., Mermoz, S., Bouvet, A., Le Toan, T., Heurich, M., 2018. Detection of windthrows and insect outbreaks by L-band SAR: A case study in the Bavarian Forest National Park. *Remote Sens. Environ.* 209, 700–711.
- Tucker, C.J., 1979. Red and photographic infrared linear combinations for monitoring vegetation. *Remote Sens. Environ.* 8, 127–150.
- White, J.C., Coops, N.C., Hilker, T., Wulder, M.A., Carroll, A.L., 2007. Detecting mountain pine beetle red attack damage with EO-1 Hyperion moisture indices. *Int. J. Remote Sens.* 28, 2111–2121.

- Wulder, M.A., Dymond, C.C., White, J.C., Leckie, D.G., Carroll, A.L., 2006. Surveying mountain pine beetle damage of forests: a review of remote sensing opportunities. *For. Ecol. Manag.* 221, 27–41.
- Wulder, M.A., White, J.C., Carroll, A.L., Coops, N.C., 2009. Challenges for the operational detection of mountain pine beetle green attack with remote sensing. *For. Chron.* 85, 32–38.
- Yang, S., 2019. Detecting bark beetle damage with Sentinel-2 multi-temporal data in Sweden. Master, Sweden.
- Yu, R., Huo, L., Huang, H., Yuan, Y., Gao, B., Liu, Y., Yu, L., Li, H., Yang, L., Ren, L., Luo, Y., 2022. Early detection of pine wilt disease tree candidates using time-series of spectral signatures. *Front. Plant Sci.* 13, 1000093.
- Yu, R., Ren, L., Luo, Y., 2021. Early detection of pine wilt disease in *Pinus tabulaeformis* in North China using a field portable spectrometer and UAV-based hyperspectral imagery. *Forest Ecosyst.* 8, 712.
- Zabihi, K., Surovy, P., Trubin, A., Singh, V.V., Jakuš, R., 2021. A review of major factors influencing the accuracy of mapping green-attack stage of bark beetle infestations using satellite imagery: prospects to avoid data redundancy. *Remote Sens. Appl. Soc. Environ.* 24, 100638.
- Zhou, H., Yuan, X., Zhou, H., Shen, H., Ma, L., Sun, L., Fang, G., Sun, H., 2022. Surveillance of pine wilt disease by high resolution satellite. *J. For. Res.* 33, 1401–1408.